Remote Sensing of Environment 305 (2024) 114114

Contents lists available at ScienceDirect

Remote Sensing of Environment

journal homepage: www.elsevier.com/locate/rse

Snow-cover remote sensing of conifer tree recovery in high-severity burn patches

Casey Menick [a,*], Wade Tinkham [b], Chad Hoffman [a], Melanie Vanderhoof [c], Jody Vogeler [d]

[a] Department of Forest and Rangeland Stewardship, Warner College of Natural Resources, Colorado State University, Fort Collins, CO 80523, USA
[b] USDA Forest Service Rocky Mountain Research Station, Fort Collins, CO 80526, USA
[c] U.S. Geological Survey, Geosciences and Environmental Change Science Center, MS 980, PO Box 25046, Denver, CO 80225, USA
[d] Natural Resources Ecology Laboratory, Colorado State University, Fort Collins, CO 80523, USA

ARTICLE INFO

Edited by Marie Weiss

Keywords:
Wildfire
Wildland fire
Landsat
Northern Rocky Mountains
Regeneration

ABSTRACT

The number of large, high-severity wildfires has been increasing across the western United States over the last several decades. It is not fully understood how changes in the frequency of large, severe wildfires may impact the resilience of conifer forests, due to alterations in regeneration success or failure. Our research investigates 30 years of conifer recovery patterns within 34 high-severity wildfire complexes (1988–1991) of the Northern Rocky Mountains. We evaluate the capability of snow-cover Landsat to characterize conifer tree recolonization of high-severity burn patches. Snow-cover images isolate conifer-specific vegetation signals by diminishing spectral contributions from soil and deciduous vegetation. The presence of conifer regeneration was successfully classified by snow-cover Landsat at >10% canopy cover at 98% accuracy and modeled at 3-year intervals post-fire. Spectral detectability of regenerating conifer vegetation began 11–19 years post-fire, varying across forest types. Thirty years post-fire, 65% of the total high-severity burn area had been recolonized by conifer trees, with differences observed between forest types: 72% of lodgepole pine, 77% of Douglas-fir, and 44% of fir-spruce severely burned areas containing conifer regeneration. Projected recovery timelines to pre-fire conifer vegetation also differed between lodgepole pine (29.5 years), Douglas-fir (36.9 years), and fir-spruce forests (48.7 years), as estimated from snow-cover NDVI trends. Although we generally documented patterns of conifer resilience, we also identified reduced likelihoods of recovery within high-severity burn patches exhibiting greater area-to-perimeter ratios, aridity, south-facing aspects, slopes, and elevation. Snow-cover Landsat imagery was shown to improve the characterization of post-fire forest recovery and may be applied to support forest restoration decision-making following high-severity wildfire.

1. Introduction

Numerous ecosystems across the globe have observed significant shifts in wildfire patterns, resulting from changes in land use, climate, fire suppression, and vegetation composition (Flannigan et al., 2009; Jolly et al., 2015; Prichard et al., 2017). Trends of increasing wildfire occurrence and extent have been well-documented across the western United States (Dennison et al., 2014; Parks and Abatzoglou, 2020; Picotte et al., 2016), notably within the Northern Rocky Mountains, a region accountable for 60% of the increase in large U.S. wildfires between 1970 and 2003 (Westerling et al., 2006). Wildfire in the Northern Rocky Mountains is anticipated to continue increasing in size and frequency, resulting from lengthening fire seasons, shortened fire return intervals, and drier fuel conditions (Morgan et al., 2008; Riley and Loehman, 2016; Westerling et al., 2011). Characteristics of wildfire severity have also shifted, with trends toward fires burning greater areas at high-severity and increasing average burn severity (Parks and Abatzoglou, 2020; Picotte et al., 2016). It is anticipated that increasing wildfire size and area burned at high-severity may reduce burn heterogeneity and create larger, more simply-shaped, high-severity burn patches (Harvey et al., 2016c).

Although fire is an important fixture in the disturbance regimes of conifer-dominated Northern Rocky Mountain forests, it is unclear how the increasing occurrence of high-severity events will impact forest resilience. Increasing prevalence of larger, more simply shaped high-severity patches may impede forest recovery by reducing access to

* Corresponding author.
E-mail address: cmenick@contractor.usgs.gov (C. Menick).

https://doi.org/10.1016/j.rse.2024.114114
Received 1 November 2023; Received in revised form 15 February 2024; Accepted 10 March 2024
Available online 16 March 2024

seed sources, as conifer seed dispersal is limited beyond 100 m from patch edges in Northern Rocky Mountain forests (Harvey et al., 2016b; Kemp et al., 2016). The ability of conifer tree species to effectively recolonize high-severity burn patches may be constrained if shortening fire return intervals preclude sufficient seed source generation (Stevens-Rumann and Morgan, 2016; Turner et al., 2019; Westerling et al., 2011). Seedling recruitment may face additional challenges with less-favorable climatic conditions for regeneration success following climate change (Stevens-Rumann et al., 2018). Forests at transitional edges in the Northern Rocky Mountains have exhibited reduced resilience to high-severity wildfire and a greater risk of conversion to non-conifer vegetation (Davis et al., 2019; Donato et al., 2016; Harvey et al., 2016c; Kemp et al., 2019; Parks et al., 2019).

Increasing wildfire activity and constrained forest recovery have many wide-ranging societal and ecological impacts. Wildfire imposes a large economic burden, costing billions of dollars annually from intervention and mitigation efforts, losses to timber and agricultural markets, and impacts on affected local communities (Bayham et al., 2022; Thomas et al., 2017). Furthermore, wildfire imposes social costs from loss of personal property, recreation opportunities, and cultural connections to natural areas (Englin et al., 1996; Gellman et al., 2022; Vukomanovic and Steelman, 2019). Ecologically, high-severity fire disrupts hydrologic patterns by increasing runoff, sedimentation, and flooding (Ice et al., 2004; Shakesby and Doerr, 2006). Soil resources are also impacted by fire effects, altering physical, chemical, and biological properties and processes (Certini, 2005; Ice et al., 2004). The loss of forest cover has implications for wildlife, altering habitat suitability and biodiversity (Fontaine and Kennedy, 2012; Steel et al., 2022). High-severity wildfire also results in increased carbon emissions and reduces the ability for forest ecosystems to sequester carbon (Loehman, 2020; Sommers et al., 2014).

It is important to characterize post-fire recovery across forest types in the Northern Rocky Mountains given the consequences of increased high-severity wildfire. Regeneration dynamics after fire are fundamental to evaluating how fire regime changes may impact forest recovery and support forest management decision-making. Post-fire regeneration densities and spatial patterns are commonly assessed through a case study approach using data covering relatively small spatial extents from plot or transect-based sampling (Chambers et al., 2016; Kashian et al., 2004; Kemp et al., 2016; Owen et al., 2017). Field studies have provided valuable information on forest recovery patterns following high-severity burns but can be limited in scope given sampling constraints. The cost of field surveys generally precludes comprehensive assessment of every fire or region, acquiring repeated measurements, or fully characterizing large areas. With millions of acres burned annually, case studies alone cannot evaluate post-fire recovery across a full spectrum of environmental conditions. Some regions cannot be assessed by field studies entirely due to remote locations, inaccessible terrain, or resource limitations. Compiling field studies to measure longitudinal or regional trends may be challenging due to differing sampling methodologies, scales, or forest conditions. National monitoring datasets, such as the U.S. Forest Service (USFS) Forest Inventory and Analysis (FIA) program (Tinkham et al., 2018), do provide long-term data on forest growth and compositional trends, but lack the necessary temporal or spectral resolution to thoroughly quantify recovery dynamics or target specific fire events. There is a need for repeat, consistent, and comprehensive data on post-fire forest recovery to adequately identify management needs and evaluate the impacts of shifting wildfire regimes.

Remote sensing has been used extensively to monitor fire effects and recovery, providing opportunities to conduct repeated monitoring over large areas (Szpakowski and Jensen, 2019). The Landsat program has been a resource for post-fire monitoring with over 50 years of consistent, freely available moderate-resolution (30 m) satellite imagery. Although there have been notable technological advances in relevant satellite spatial (e.g., Sentinel, WorldView; Howe et al., 2022; Wu et al., 2015) and spectral resolution (e.g. ASTER, AVIRIS; Holden et al., 2010; Van Wagtendonk et al., 2004), Landsat remains one of the most widely used tools to monitor post-fire recovery given its accessibility and availability (Chuvieco et al., 2020; Szpakowski and Jensen, 2019). Typical post-fire remote sensing assessments measure recovery as a return to pre-fire growing-season vegetation greenness, with spectral indices such as the Normalized Difference Vegetation Index (NDVI; Szpakowski and Jensen, 2019; White et al., 1996). Spectral indices including the Normalized Burn Ratio (NBR; Bright et al., 2019; Frazier et al., 2018), Enhanced Vegetation Index (EVI; Casady et al., 2010), Disturbance Index (Chen et al., 2014), and Forest Recovery Index 2 (Morresi et al., 2019) have also been used to track post-fire recovery, however, NDVI is popular because it is highly correlated with canopy photosynthetic capacity and chlorophyll abundance (Myneni et al., 1995). Although growing-season spectral indices are a useful measure of vegetation density and greenness, they are generally not sensitive to vegetation species assemblages or growth form. The lack of specificity in growing-season NDVI, for instance, may overestimate rates of post-fire forest recovery by conflating the presence of vegetation with the re-establishment of coniferous tree cover (Bright et al., 2019; Kiel and Turner, 2022; Vanderhoof and Hawbaker, 2018).

Several remote sensing analyses have found success utilizing phenologically-informed seasonal imagery to differentiate between forest vegetation types (Dymond et al., 2002; Kiel and Turner, 2022; Townsend and Walsh, 2001; Wang et al., 2022; Wolter et al., 1995). Winter imagery has been shown to specifically improve the discrimination of evergreen conifer (hereafter *conifer*) tree presence from other vegetation (Vanderhoof et al., 2021; Wolter et al., 2008). By using snow cover as a physical and phenological filter, spectral contributions of vegetation greenness from deciduous, herbaceous, and low-lying evergreen vegetation are diminished. Snow-cover imagery has been successfully utilized to measure post-fire conifer NDVI trends (Vanderhoof et al., 2021; Vanderhoof and Hawbaker, 2018), but has not yet been applied to spatially map regenerating conifer vegetation following wildfire. Utilizing snow-cover imagery to assess the spatial progression of conifer regeneration can create a more detailed picture of post-fire recovery that describes the proportion of burn patches reforested by conifer species. Pixel-based binary classification of conifer presence or absence has the potential to describe post-fire dynamics typically only achieved with field studies, but with the larger temporal and spatial scales of Landsat.

Our study applies snow-cover Landsat imagery to spatially characterize conifer regeneration following high-severity wildfires in the Northern Rocky Mountains. We focus on 34 high-severity wildfire complexes (1988–1991) that occurred following the 1988 North American Drought (Trenberth et al., 1988). This series of fire events includes 7 of the 38 extreme fire events occurring in the Northern Rocky Mountains and Great Basin between 1984 and 2009 (Lannom et al., 2014). We compare 30 years of conifer regeneration patterns following high-severity burns for several conifer-dominated forest types in the Northern Rocky Mountains. Our research objectives are to:

1. Evaluate the ability of Landsat and snow-cover remote sensing to detect conifer regeneration.
2. Characterize conifer recolonization and estimate recovery timelines following high-severity wildfire across forest types within the Northern Rocky Mountains.
3. Identify site characteristics of high-severity burn patches that impact the likelihood of successful conifer recovery 30-years post-fire in the Northern Rocky Mountains.

2. Methods

2.1. Study area

The study area was defined as the U.S. Northern Rocky Mountains, comprised of four, conifer-dominated U.S. Environmental Protection

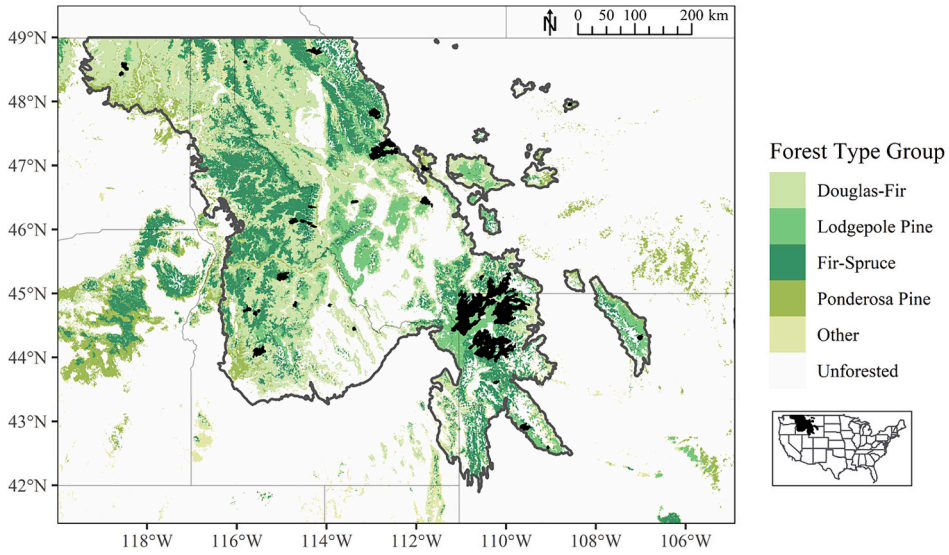

Fig. 1. Study area map of the 34 high-severity fire events used in our analysis, with fire extents highlighted in black. The dark gray boundary line indicates the combined area of the U.S. portion of the Environmental Protection Agency Level-III Ecoregion groups Canadian Rockies, Northern Rockies, Middle Rockies, and Idaho Batholith (Omernik and Griffith, 2014). Dominant forest types from the U.S. Forest Service National Forest Type Group Dataset are shown in shades of green (Ruefenacht et al., 2008). (For interpretation of the references to colour in this figure legend, the reader is referred to the web version of this article.)

Agency (EPA) Level-III Ecoregion groups: Canadian Rockies, Northern Rockies, Middle Rockies, and Idaho Batholith (Omernik and Griffith, 2014). The four ecoregions encompass portions of Idaho, Montana, Wyoming, and Washington states (Fig. 1). At higher elevations, the forests of our study area are comprised of subalpine forests dominated by subalpine fir (*Abies lasiocarpa*) and Engelmann spruce (*Picea engelmannii*) commonly associated with lodgepole pine (*Pinus contorta*) and whitebark pine (*Pinus albicaulis*). Lower to mid-elevation mixed-conifer forests are comprised primarily of Douglas-fir (*Pseudotsuga menziesii*) alongside western larch (*Larix occidentalis*), grand fir (*Abies grandis* var. *idahoensis*), ponderosa pine *(Pinus ponderosa)*, limber pine (*Pinus flexilis*), lodgepole pine, and quaking aspen (*Populus tremuloides*) (Daubenmire, 1943).

2.2. Fire selection

Candidate fires were identified within the Northern Rocky Mountains using Monitoring Trends in Burn Severity (MTBS) fire perimeter datasets (Eidenshink et al., 2007). Fires occurring between 1988 and 1991 were selected to assess regeneration over a 30-year post-fire period and ensure a sufficient record of pre-fire Landsat imagery. Fires were excluded from analysis if <25% of the burned area represented a coniferous forest type of interest using the USFS National Forest Type Group dataset (Ruefenacht et al., 2008). Relevant forest types included Douglas-fir, ponderosa pine, fir-spruce-mountain hemlock (hereafter *fir-spruce*), and lodgepole pine. The MTBS thematic burn severity dataset was utilized to select fire events with at least 200 ha of high-severity burning to facilitate relevant comparisons between patch sizes and forest types. After evaluating candidate fire suitability, ponderosa pine forests were excluded from further analysis with an insufficient area of high-severity fire identified (< 2000 ha). We likely found limited high-severity fire events within ponderosa pine due to historically lower-severity fire regimes (Schoennagel et al., 2004) and overall lower prevalence across the study region (Fig. 1).

For each candidate fire, we excluded all areas within burn perimeters that would not exhibit patterns of natural regeneration due to management activity or reburning. Areas were removed from analysis if they showed evidence of notable human activity or silvicultural management, such as road systems, buildings, or planting rows during visual inspection of high-resolution satellite imagery. Where applicable, fire perimeters were cross-referenced with the USFS Forest Activity Tracking System (FACTS) dataset of reforestation activities to remove areas of known planting or regeneration site preparation on federal lands. Areas of reburning were also excluded from analysis after comparison to the MTBS fire perimeter dataset. Fire selection criteria resulted in a final dataset of 34 high-severity wildfire complexes within the Northern Rocky Mountains, corresponding to 47 MTBS-defined events and 890,000 ha of area burned.

2.3. Identification of high-severity burn patches

High-severity burn patches were identified within the 34 wildfire complexes using the Landsat-derived Relative differenced Normalized Burn Ratio (RdNBR) (Miller and Thode, 2007). RdNBR is a spectral burn severity index based on the Normalized Burn Ratio (NBR), which calculates the ratio of wavelengths sensitive to the presence of vegetation and burned areas, near-infrared (NIR) and short-wave infrared (SWIR) (Eq. (1); Key and Benson, 2006; White et al., 1996). Burn severity is typically determined by differencing NBR values before and after a fire event, with larger differenced NBR (dNBR) values corresponding to more severe fire effects (Szpakowski and Jensen, 2019). RdNBR improves upon dNBR by relativizing spectral values by pre-fire vegetation condition, improving the classification of burn severity across heterogeneous forests (Eq. (2); Cansler and McKenzie, 2012; Miller et al., 2009; Pelletier et al., 2021). Relativizing burn severity particularly improves the classification of areas burned at high-severity, as the measure more accurately corresponds to near-total vegetation loss (Miller and Thode, 2007). Although MTBS data were used to initially identify high-severity fire events, the reliance on analyst interpretation to set dNBR thresholds is known to cause finer-scale issues when comparing multiple fires (Kolden et al., 2015; Sparks et al., 2014) or evaluating historic fire events where precise field data were often limited for classification (Miller and Thode, 2007).

$$NBR = \frac{NIR - SWIR}{NIR + SWIR} \tag{1}$$

$$RdNBR = \frac{NBR_{prefire} - NBR_{postfire}}{\sqrt{|NBR_{prefire} \times 0.001|}} \tag{2}$$

Burn severity was calculated from RdNBR by adapting the approach described by Parks et al. (2018). Pre- and post-fire imagery were

compiled from the mean annual composite of growing season (day 152–273) Landsat 5 Thematic Mapper (TM) Surface Reflectance imagery for one year before and after each fire event. The utilization of annual composites has been shown to improve burn severity classification accuracy relative to individual scene selection by standardizing imagery, removing the necessity of analyst image selection, and reducing potential errors from reliance on a singular image (Parks et al., 2018). Annual composites using imagery from one full year before and after a fire event perform well in western U.S. conifer forests by standardizing vegetation conditions between fires and accounting for delayed mortality. To address potential phenological differences between the pre- and post-fire imagery, we calculated a dNBR offset adjustment based on the mean dNBR value for all unburned pixels within a 180 m buffer around the fire perimeter. High-severity pixels were identified using RdNBR values >640, a threshold associated with 95% or greater tree mortality in field-collected data from similar forests (Haffey et al., 2018; Hanson and Odion, 2014; Miller and Thode, 2007).

Individual high-severity burn patches were delineated using the 'patchMorph' tool from the 'patchwoRk' package (Girvetz and Greco, 2007) in the R statistical program (R Core Team, 2021). The tool created patch polygons from contiguous high-severity burn pixels using 3-cell (90 m) separation thresholds for spurs and gaps between patches. Focal filtering has been shown to improve burn severity classification, reduce pixelation, and create more ecologically relevant patches (Collins and Stephens, 2010; Miller et al., 2012; Pelletier et al., 2021; Stevens et al., 2021). Patches were assigned to the majority forest type group present as defined by the USFS National Forest Type Group dataset (Ruefenacht et al., 2008). Any patches smaller than 2.25 ha, equivalent to 25 Landsat pixels at 30 m resolution, were excluded from our analysis. Through our selection process, we obtained a final dataset of 3850 high-severity burn patches, totaling nearly 300,000 ha, for analysis.

2.4. Snow-cover Landsat imagery

Snow-cover imagery was assembled from Google Earth Engine Landsat 5, 7, and 8 Surface Reflectance data to track conifer-specific vegetation recovery. Images were selected from a range of winter months (December–April) that would reliably be snow-covered and provide a temporal window that would ensure image availability given challenges posed by seasonal cloud cover. For each selected image, several spectral indices associated with vegetation, moisture, burn severity, and snow-cover were calculated: the Normalized Difference Vegetation Index (NDVI; Tucker, 1979), the Enhanced Vegetation Index (EVI; Huete et al., 2002), the Normalized Difference Water Index (NDWI; Gao, 1996), the Normalized Burn Ratio (NBR; García and Caselles, 1991), the Normalized Burn Ratio 2 (NBR2; Key and Benson, 2006), the Normalized Difference Snow Index (NDSI; Hall and Riggs, 2010), and the Normalized Difference Forested Snow Index (NDFSI; Wang et al., 2015). Pixels containing cloud, cloud shadow, or bodies of water were excluded utilizing Landsat's Quality Assurance (QA) bands.

Although the study area is regularly snow-covered within the selected winter months, an image-masking process was applied to ensure pixels were representative of true snow-cover conditions. From the winter imagery, pixels were only retained for analysis if they had NDFSI or NDSI values >0.4, spectral thresholds that are strongly correlated with the presence of snow in forested and unforested areas, respectively (Hall et al., 1995; Wang et al., 2015). Spectral indices NDSI and NDFSI can identify the presence of snow by comparing the ratio of visible and NIR light, respectively, to SWIR radiation, which exhibits very low reflectance over snow. NDSI is used as the global standard for detecting snow coverage (Riggs et al., 2017), with improved performance in conifer forests using NDFSI (Wang et al., 2015). Our methodology enables an automated approach to flexibly select snow-covered imagery and effectively buffer against irregular annual snow coverage.

Composite images were created for each winter season (December–April) by calculating the median pixel values of the masked Landsat images. Median image composites help minimize the influence of irregular snow-cover and the effect of potential spectral outliers. Our process of image selection and compositing resulted in an annual series of 13-band images, including six spectral bands and seven derived indices, for each fire event between 1984 and 2021. The collection of annual snow-cover image composites underwent a series of spectral analyses to characterize conifer recovery within high-severity burn patches over time (Fig. 2).

2.5. Snow-cover NDVI trends

To track post-fire conifer spectral recovery, patterns of snow-cover NDVI were evaluated through time. Snow-cover NDVI corresponds to coniferous vegetation by evaluating vegetation greenness when conifers represent the predominant spectral signal (Vanderhoof et al., 2021). Annual snow-cover NDVI values were calculated for each high-severity burn patch by averaging all respective pixel values. Each NDVI value was normalized to differenced NDVI (dNDVI) using the mean pre-fire snow-cover NDVI value for each individual burn patch to better evaluate the relative change in vegetation greenness. We applied a piecewise generalized linear regression using the 'segmented' package in R (Muggeo, 2008) to analyze trends in snow-cover dNDVI through time. Piecewise regression was employed to identify when a positive dNDVI slope occurred post-fire, signifying a detectable increase in vegetation greenness assumed to represent coniferous regeneration. The mean annual dNDVI values from all high-severity burn patches ($n = 3850$) were used by the model. The model was set to identify one breakpoint, using years post-fire as a predictor of snow-cover dNDVI for each forest type. Linear trends from the piecewise regressions were used to estimate the post-fire dNDVI recovery rates and timelines within each forest type. Recovery timelines were calculated as the estimated number of years to reach pre-fire snow-cover NDVI values, indicating that a high-severity burn patch had returned to initial conifer vegetation greenness values.

2.6. Modeling conifer presence and absence

A Random Forest classification model was developed using the R package 'randomForest' (Liaw and Wiener, 2002) to evaluate the spatial progression of conifer recolonization through time. The model was built to classify all pixels within the high-severity burn patches as either present or absent of conifer tree species at timepoints throughout the 30-year post-fire recovery period. Random Forest classifiers are non-parametric and work well with the classification of remotely sensed imagery as they do not rely on normally distributed data and are less susceptible to overfitting (Belgiu and Drăguţ, 2016).

Model training points were distributed across high-severity patches, with 100 training points allocated to each of the 47 MTBS fire events ($n = 4700$). Training points were randomly assigned, with a minimum separation of 30 m, and equal stratification between north and south aspects and patch exterior and interior. Stratification by aspect was implemented to account for potential spectral differences from solar angle. Stratification by patch interior and exterior was applied to increase the likelihood of the post-fire training data including more equivalent proportions of regenerating conifer presence and absence. Patch interior was conservatively defined as ≥150 m from patch edges, based on probable seed dispersal distances from surviving forest edges (Kemp et al., 2016). Training points were intersected with a 30 m fishnet grid aligned with the snow-cover Landsat pixels and visually categorized as either present or absent of conifers utilizing a combination of the most recently available 1 m resolution National Agricultural Imagery Program (NAIP) and high-resolution (0.3–1 m) imagery available in Google Earth. Several late-season NAIP acquisition years provided at least one snow-cover image for most fire events, which offered useful comparisons of deciduous and coniferous vegetation. Pixel values were obtained for each training point from the average of three annual snow-cover Landsat composites (2018–2021) to ensure data availability and

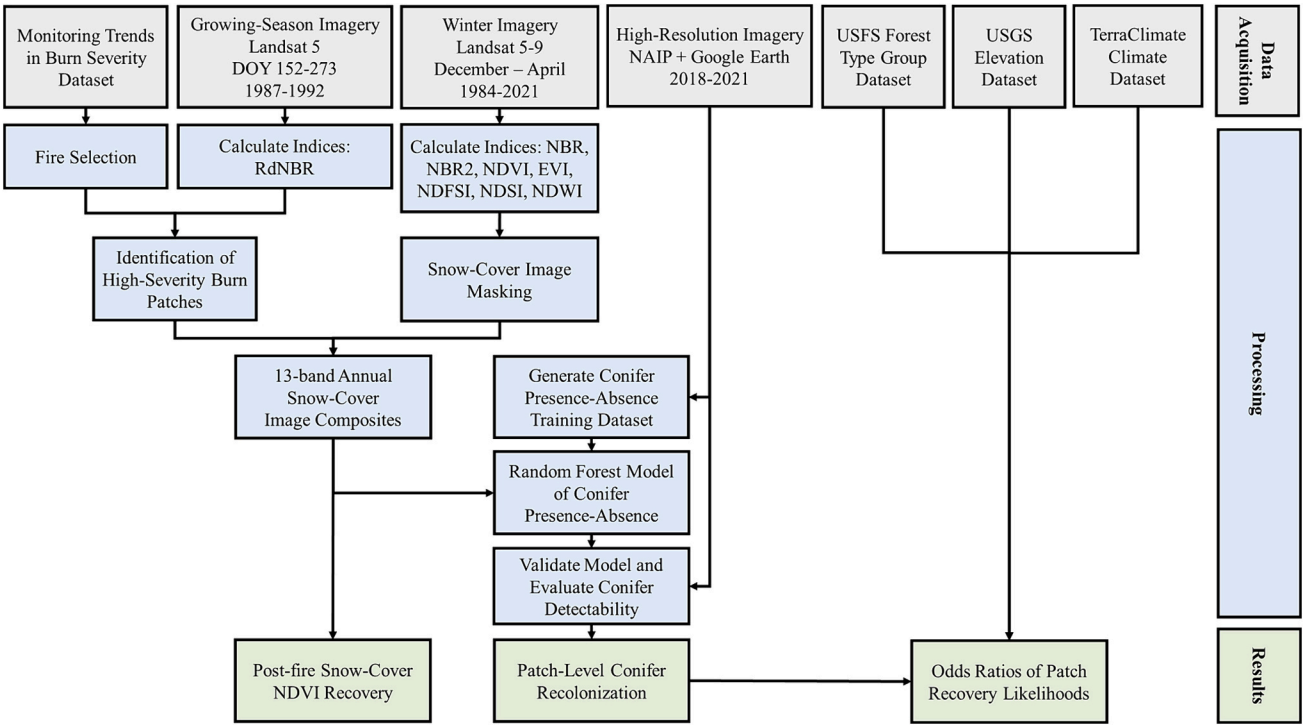

Fig. 2. Diagram showing the methodological workflow followed by our study design. Initial data inputs, processing steps, and final study results are documented. DOY: day of year, NAIP: National Agriculture Imagery Program, USFS: U.S. Forest Service, USGS: U.S. Geological Survey, NBR: Normalized Burn Ratio, RdNBR: Relative differenced NBR, NDVI: Normalized Difference Vegetation Index, EVI: Enhanced Vegetation Index, NDFSI: Normalized Difference Forested Snow Index, NDSI: Normalized Difference Snow Index, NDWI: Normalized Difference Water Index.

account for potential variation in annual snow-cover. The model was trained with 2018–2021 Landsat imagery to align with the high-resolution imagery used to identify conifer cover and capture the widest range of vegetation conditions across the landscape. The Random Forest model used the 13 snow-cover Landsat spectral bands from the training data points as predictors of conifer presence or absence. The number of predictors tried at each split (*mtry*) was set at three and the number of trees (*ntrees*) evaluated was 500.

The model was independently validated using 20 validation points per MTBS event, randomly distributed with stratification by conifer presence and absence classes. A minimum distance of 30 m was enforced between points and from training points, to enable adequate validation points in smaller burned patches. The mean distance between validation and nearest-neighbor training points was 558 m. For each MTBS event, 10 points were allocated between classes proportionally by predicted area with an additional 5 points allotted to each class to ensure a sufficient minimum validation sample size (Olofsson et al., 2014). Validation points ($n = 940$) were visually classified as conifer present or absent using the same high-resolution imagery used to train the model, with a 30 m fishnet grid overlaid. The performance of the classification was evaluated in a confusion matrix comparing the actual target classes against those predicted by the model. Additional post-model testing was conducted to assess the potential influence of spatial autocorrelation between training and validation datasets on model performance (Kattenborn et al., 2022). First, we compared model accuracies for the full validation dataset against a subset where validation points within 100 m of a training point were withheld, a threshold distance regularly used to avoid spatial autocorrelation in similar studies (White et al., 2022). Chi-squared tests were used to evaluate differences in model performance for validation points that were nearer to or further from training data points using several distance benchmarks (60 m – 600 m).

Misclassified validation points were leveraged to characterize the detectability of conifer regeneration within a Landsat pixel. For the subset of validation pixels that contained conifer trees but were incorrectly classified as conifer absent ($n = 149$), the proportion of conifer canopy cover was evaluated. These misclassified validation pixels indicate where the model is not performing well and can be used to identify a threshold of conifer cover that cannot be identified accurately by our methodology. Canopy cover was calculated by counting the proportion of 1 m NAIP grid cells containing conifer trees that overlaid each misclassified 30 m Landsat pixel.

After validation, the model was applied through time to characterize conifer recolonization of the high-severity burn area. The snow-cover Landsat imagery was aggregated into 10 timepoints by computing the mean value of the annual composites at three-year intervals. Consistent with the model training and validation data, three-year composites were used to ensure data availability and control for annual snow-cover variability. For each timestep, the model was used to predict conifer presence or absence, resulting in 10 conifer presence-absence rasters spanning the 30-year recovery period following each fire event. The proportion of conifer-present pixels was assessed for all high-severity burn patches at each analysis timestep.

2.7. Identifying characteristics of recovery

Factors associated with an increased likelihood of successful conifer recovery 30 years post-fire were identified from high-severity burn patch characteristics. Recovery success was defined as a high-severity patch reaching 80% conifer recolonization, a threshold corresponding to near-intact forest structure (Viana-Soto et al., 2022; White et al., 2017). A generalized linear logistic regression model was created using the R package 'rms' (Harrell Jr, 2013) to predict patch recovery. A suite of predictor variables was calculated for all high-severity patches to characterize significant ($p < 0.05$) biological and environmental controls on forest recovery. Forest type was used as a categorical predictor to account for inherent differences in recovery timelines among forest ecosystems. Patch area and area-to-perimeter ratio were included to describe the importance of patch size and configuration. Climate water

deficit (DEF) was used to characterize evaporative demand, calculated as the mean patch value from TerraClimate data (Abatzoglou et al., 2018) in a 3-year window (1985–1987) before the fire events occurred. The influence of topographic variables was assessed from the mean patch slope, cosine-corrected aspect, and elevation derived from the 'elevatr' R package (Hollister et al., 2021). Cosine-correction of aspect provides an estimate of 'northness', with values close to 1 representing north-facing aspects, and values close to −1 representing south-facing aspects. Odds-ratios were calculated for all predictors to assess the relative impact of each on conifer recovery likelihood. The change in odds-ratios across the interquartile range of each predictor was also determined to provide more relevant comparisons between variables.

3. Results

3.1. High-severity burn patch distributions

Following the high-severity burn patch identification process, a final dataset of 3850 high-severity burn patches were identified (Table 1). The burn patch dataset represents 34 high-severity wildfire complexes, with varying distributions of patch sizes and forest composition. Over 51% of the high-severity burn patches were located within lodgepole pine forests, with 37% and 11% in the fir-spruce and Douglas-fir forest types, respectively. By area, lodgepole pine represented 72%, fir-spruce 22%, and Douglas-fir 6%. Across all forest types, relatively small (<50 ha) patches accounted for the majority (87%) of the total number of patches, yet only represented 11% of the total area burned at high-severity. Conversely, a few very large (>1000 ha) patches represented a disproportionate amount (57%) of the high-severity burn area. Douglas-fir and fir-spruce had more similar distributions of patch number and area between the size classes, whereas lodgepole pine had a much larger proportion of area (69%) within the largest (>1000 ha) size class.

3.2. Snow-cover dNDVI recovery and detection

The piecewise generalized linear regression of post-fire snow-cover dNDVI had adjusted R^2 values of 0.96 and 0.90 for Douglas-fir and lodgepole pine respectively, whereas fir-spruce showed greater variability along the trendline with an adjusted R^2 of 0.58 (Fig. 3). All three forest types saw similar reductions to snow-cover dNDVI post-fire, with model intercepts between −0.162 and − 0.193. Initial snow-cover dNDVI slopes were slightly negative for all forest types before the breakpoint, varying between −0.0032 and − 0.0013, although the slope was only significant ($p < 0.05$) for fir-spruce. The segmented model breakpoints (hereafter *detection points*) differed by forest type, at 11.5 years for Douglas-fir, 14.6 years for lodgepole pine, and 19.4 years for fir-spruce. Post-detection slopes were all significantly positive ($p < 0.05$), and greatest in lodgepole pine at 0.0124, followed by 0.0082 in Douglas-fir, and 0.0076 in fir-spruce. If future dNDVI trends continue to follow the linear post-detection slope, the estimated recovery time to pre-fire snow-cover NDVI values would be 29.5 years in lodgepole pine, 36.9 years in Douglas-fir, and 48.7 years in fir-spruce.

3.3. Conifer presence-absence model performance and recovery trends

The conifer presence-absence Random Forest model had an initial estimated out-of-bag error rate of 12.0%. The variables of highest importance to the model were the spectral indices NDVI, NDWI, NBR2, and NBR. Accuracy assessment through independent validation showed an overall accuracy rate of 83.2%, with 98.8% accuracy at classifying conifer presence and 58.9% accuracy at classifying conifer absence (Table 2). We found no evidence to indicate that spatial autocorrelation influenced model accuracy, with similar overall performance (82.4%) excluding validation points within 100 m of a training point. Further, chi-squared tests showed that model performance was insignificantly different between all tested training point nearest-neighbor distance thresholds.

For misclassified validation pixels, where conifer trees were present in the reference class but were incorrectly classified as absent, we found that the majority (72%) of the Landsat pixels had <10% coniferous tree cover (Fig. 4). A forest canopy cover of 10% corresponds to the definitions of 'forested' used by the USFS FIA and United Nations Food and Agriculture Organization (Gray et al., 2012; Food and Agriculture Organization of the United Nations, 2020), indicating that the majority of false negatives occurred where conifer trees were present within an unforested condition. The overall difference in class-level accuracies we documented indicates that our classification of conifer presence may be more conservative than what is present on the landscape.

Conifer recolonization was characterized by tracking the proportion of modeled conifer-present pixels over time for all high-severity burn patches (Fig. 5). Thirty years post-fire, conifer trees had recolonized 65% of the total high-severity area burned (Fig. 6). The proportion of total area occupied by conifer trees varied by forest type: 72% of lodgepole pine, 77% of Douglas-fir, and 44% of fir-spruce forests.

The distribution of conifer recolonization across each of the 3850 high-severity burn patches was also evaluated over time. Similar reforestation trajectories were observed for Douglas-fir and lodgepole pine patches, with median proportions of conifer occupancy after 30 years of 91.1% and 100%, respectively (Fig. 5). Lodgepole pine exhibited more consistent conifer recovery across all patches, with an interquartile range of proportional area occupied by conifer trees of 9.8% compared to 46.3% in Douglas-fir. In contrast, fir-spruce patches displayed a slower rate of conifer recolonization, achieving a median conifer occupancy of 41.3% after 30 years, and demonstrated greater variation in recovery across patches, with an interquartile range of 62.3%.

3.4. Evaluation of patch recovery

Odds-ratios of patch characteristics associated with conifer recovery were identified (Table 3). Forest type had a significant effect ($p < 0.001$) on determining conifer recovery, with lodgepole pine and Douglas-fir patches, respectively, associated with a 6.0- and 2.0-times greater likelihood of patch recovery relative to fir-spruce. Lodgepole pine also had a 3.0-times greater likelihood of recovery compared to Douglas-fir. Increasing patch area-to-perimeter ratio, climate water deficit, elevation, and slope, along with decreasing aspect northness were significantly associated ($p < 0.001$) with lower likelihoods of conifer recovery. Patch area was not found to have a significant effect on conifer recovery ($p > 0.05$).

Table 1
Distribution of the number and area of high-severity burn patches evaluated within the study area. Patches are arranged by U.S. Forest Service forest type groups Douglas-fir, fir-spruce, and lodgepole pine and by patch size class.

	<50 ha		50–100 ha		100–500 ha		500–1000 ha		>1000 ha	
Forest Type Group	Area (ha)	*n*	Area (ha)	*n*	Area (ha)	*n*	Area (ha)	*n*	Area (ha)	*n*
Douglas-fir	3633	387	1778	25	4891	21	1457	2	5886	3
Fir-spruce	11308	1246	4593	67	17857	82	12422	16	16225	7
Lodgepole pine	15509	1725	7756	112	22590	109	16768	24	139421	23

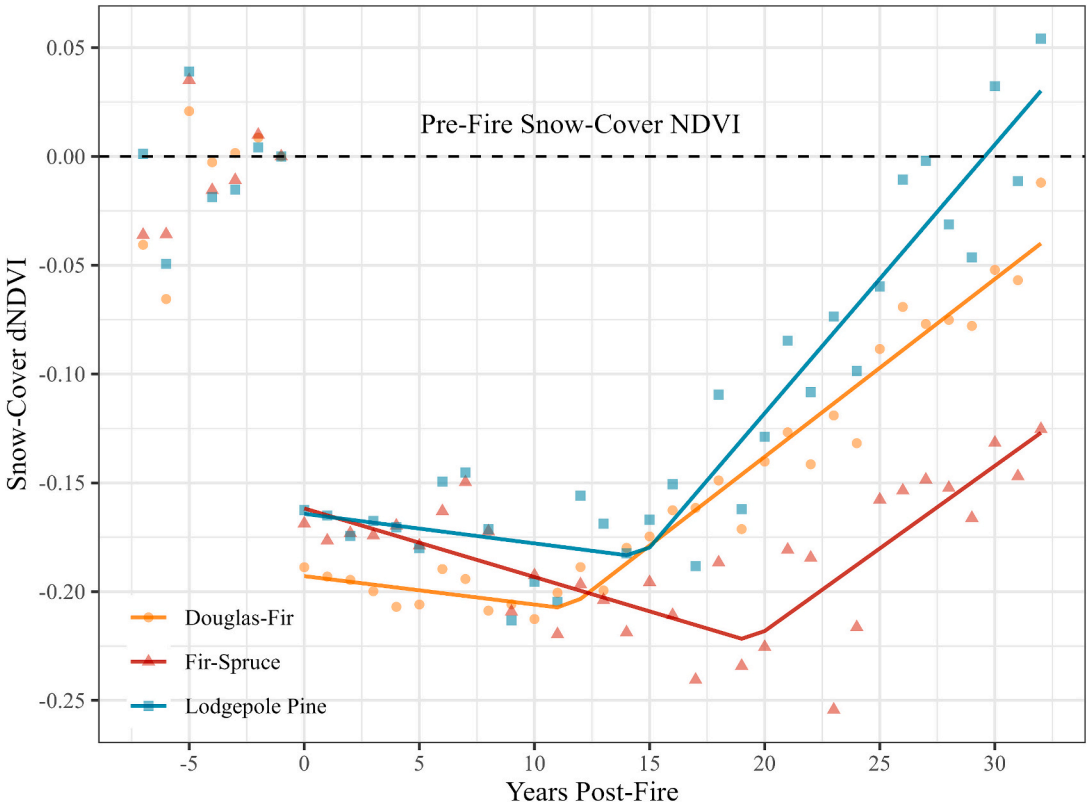

Fig. 3. Piecewise generalized linear regression of snow-cover differenced Normalized Difference Vegetation Index (dNDVI) through time, comparing Douglas-fir, lodgepole pine, and fir-spruce forest type groups. Each point represents the mean snow-cover dNDVI value across all high-severity burn patches for each forest type. Snow-cover NDVI values were relativized by pre-fire vegetation condition for all high-severity burn patches and plotted through time relative to the fire event year.

Table 2
Conifer presence-absence Random Forest model error matrix from independent validation expressed in terms of proportion of total area represented by each class. Total (W_i) represents the mapped area proportions of each class. U_i and P_i characterize the user's and producer's accuracy of each class, respectively.

Map Classification	Reference Class				
	Conifer Presence	Conifer Absence	Total (W_i)	U_i	P_i
Conifer Presence	0.650	0.008	0.658	98.8%	77.6%
Conifer Absence	0.140	0.202	0.342	58.9%	96.8%

To demonstrate the relative performance of each continuous predictor variable within our study area, we compared the relative change in odds ratios across the interquartile range for each variable. Topographic variables had the largest odds-ratio magnitude across the interquartile range of the data, with a 64% and 74% reduction in the likelihood of conifer recovery as elevation and slope increased, respectively, and a 59% decrease going from northern to southern aspects. Other predictors showed a 17% reduction in recovery odds across climate water deficit and 16% reduction in recovery odds across area-to-perimeter ratio.

4. Discussion

4.1. Snow-cover remote sensing performance and application

Our study supports the capability of snow-cover NDVI trends to assess post-fire conifer recovery, consistent with previous research (Vanderhoof et al., 2021; Vanderhoof and Hawbaker, 2018). Piecewise regression of post-fire dNDVI furthered prior efforts, estimating snow-cover Landsat conifer detection limits (~10% canopy cover) and post-fire conifer recovery timelines (30–49 years post-fire) within high-severity burn patches. Furthermore, snow-cover imagery was proven to be an effective technique to spatially identify the presence of regenerating coniferous tree cover, with over 98% classification accuracy. Although our methods were ineffective at detecting low conifer cover, this implies that our classification is more analogous to forested levels of coniferous vegetation, rather than the presence of individual conifer trees. Other studies have similarly employed a 10% cover threshold to evaluate forest recovery (Bartels et al., 2016; White et al., 2018; Zhao et al., 2016) and found similar thresholds of vegetation cover detectability within Landsat pixels (Negrón-Juárez et al., 2011; Sankey and Glenn, 2011; Williams and Raymond, 2002). Mapping conifer-specific forest cover through a pixel-based approach is a powerful tool to characterize post-fire vegetation recovery. Alongside snow-cover NDVI, the mapped extent of conifer cover can be used to identify areas of regeneration failure and directly inform forest management decision-making following high-severity wildfire. Spatially representing conifer regeneration has the potential to inform other aspects of recovery, such as predicting hydrological responses (Niemeyer et al., 2020; O'Donnell et al., 2018, evaluating wildlife habitat suitability (Ackers et al., 2015; Nelson and Buech, 1996), and estimating carbon sequestration (Kashian et al., 2006; Meigs et al., 2009). Understanding post-fire stand development is crucial to address challenges posed by the increasing occurrence and extent of high-severity wildfires in the western United States. There remains a need for long-term research on conifer recovery patterns, particularly in fire-prone ecosystems with limited field studies or at an increased risk of regeneration failure.

Although snow-cover Landsat was proven to be successful for our applications, we identified potential limitations and opportunities for

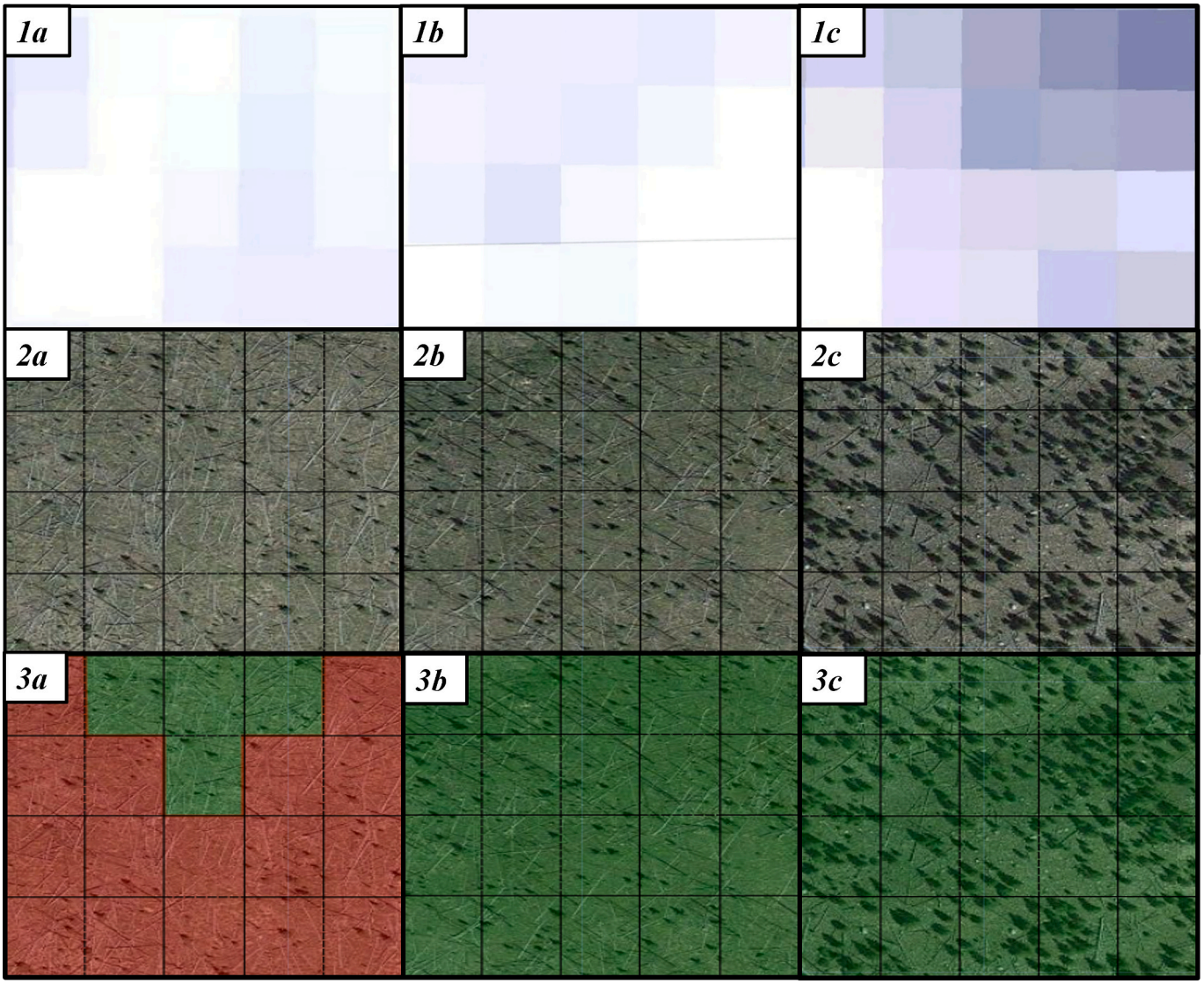

Fig. 4. Examples of (*1*) true-colour snow-cover Landsat imagery, (*2*) high-resolution satellite imagery used to develop conifer presence-absence model training data, and (*3*) overlayed classified conifer presence-absence Random Forest model output with predicted conifer presence in green and absence in red for three levels of conifer tree cover (*a-c*). (*a*) illustrates low (<10%) conifer cover and subsequent model misclassification as conifer absence. (*b*) represents low, but detectable levels of conifer cover and (*c*) shows high levels of conifer cover, both of which are correctly classified by the model as conifer presence. (For interpretation of the references to colour in this figure legend, the reader is referred to the web version of this article.)

future development. Modeling conifer presence post-fire may be hindered in study systems with low densities of conifer trees or irregular winter snow-cover. Higher resolution satellites may reduce the delay before regeneration becomes detectable or improve performance in low conifer cover systems by enabling more precise aerial estimation of conifer presence, particularly if the spatial resolution allows a single tree to correspond to >10% pixel coverage. Incorporating other remotely-sensed data sources, such as LiDAR, additional spectral bands, or additional imagery timepoints could also feasibly enhance the ability to detect conifer vegetation presence. Considering local vegetation composition and snow-cover extent, timing, and depth during the image selection process may also improve conifer detection by having a higher proportion of vegetation visible. Study areas with sparse winter snow-coverage could explore integrating leaf-off imagery to separate coniferous vegetation signals (Kiel and Turner, 2022; Townsend and Walsh, 2001). Designing region-specific modeling approaches, with unique image selection processes dependent on winter seasonality and vegetation composition, may be a desirable approach. Where these methodological adjustments are unable to sufficiently increase model performance, considering the overall change in snow-cover NDVI, rather than explicitly mapping conifer cover, may be a preferable alternative.

Unaided, our methods cannot evaluate the recovery of deciduous conifer (i.e., *Larix* spp) or broadleaf tree species, or identify compositional shifts in coniferous species dominance. Combining growing-season and snow-cover imagery may offer opportunities to assess recovery for both evergreen conifer and deciduous vegetation (Vanderhoof et al., 2021). Future studies using snow-cover imagery could incorporate other datasets to evaluate forest structural or compositional recovery. Prior research has successfully integrated LiDAR with Landsat imagery to measure both spectral and structural vegetation recovery (Bolton et al., 2015; McCarley et al., 2017; Szpakowski and Jensen, 2019; Viana-Soto et al., 2022; Wulder et al., 2009). Others have paired moderate resolution imagery with field collected data, such as FIA, to identify forest composition across broad spatial scales (Obata et al., 2021; Ruefenacht et al., 2008; Song et al., 2007; Thapa et al., 2020; Tinkham et al., 2018).

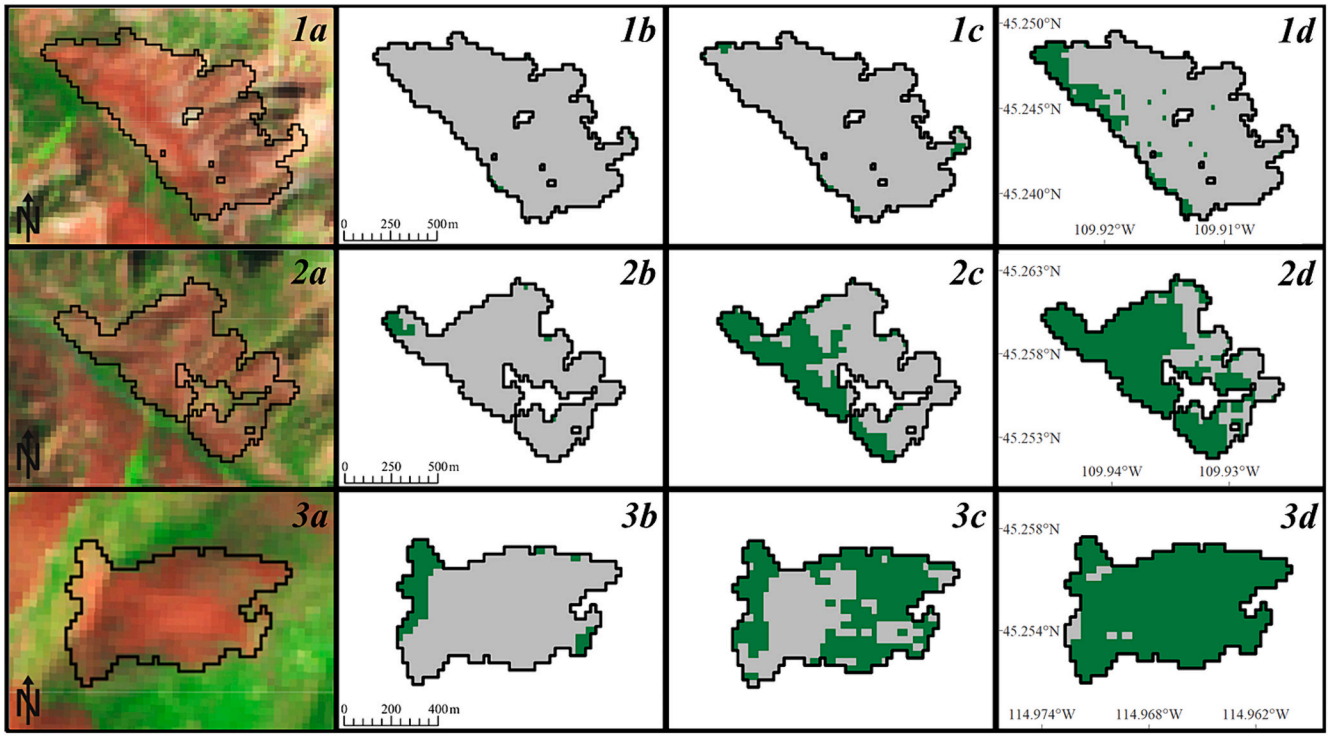

Fig. 5. Examples of the conifer presence-absence modeling for three high-severity burn patches, representing minimal (*1*), moderate (*2*), and full (*3*) conifer recovery scenarios. Panel *a* shows Landsat 5 Thematic Mapper imagery using a false colour composite (bands 7, 4, 3) immediately following each fire event and the extent of each high-severity burn patch. Panels *b-d* show mapped conifer presence in green at three points along the timeseries, associated with year 10, 20, and 30 post-fire, respectively. (For interpretation of the references to colour in this figure legend, the reader is referred to the web version of this article.)

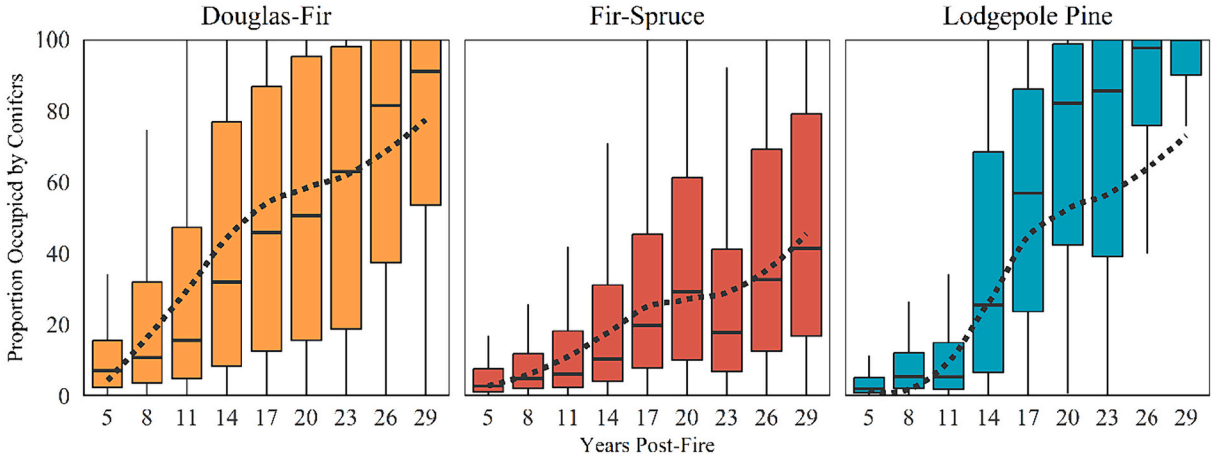

Fig. 6. Boxplot distributions of the proportion of conifer occupancy across all high-severity burn patches at 3-year analysis time timepoints for each forest type group. Dotted trendlines represent the cumulative distribution of the proportion of area occupied by conifer trees across all high-severity burn patches.

4.2. Patterns of snow-cover NDVI

The patterns of snow-cover dNDVI show progression toward forest recovery across high-severity burn patches, relaying the amount of vegetation greenness relative to the initial forest stand conditions. Increases in the proportion of conifer recolonization we documented generally align with the trends observed in snow-cover dNDVI. The variation in dNDVI between the three forest types through time aligns with the mean patch recolonization through time. Lodgepole pine regeneration typically occurs in a singular pulse in the year following a fire event, with serotinous cones releasing seed en masse, followed by relatively rapid seedling growth. Conversely, Douglas-fir, Engelmann-spruce, and subalpine fir rely on seed dispersal from surviving parent trees, leading to more prolonged seedling establishment peaking 4–6 years post-fire (Harvey et al., 2016c). Seed dispersal is generally constrained to 100 m within surviving parent trees in Northern Rocky Mountain forests (Gill et al., 2021; Kemp et al., 2016), potentially requiring several successive generations of seedling recruitment, growth, and dispersal to recolonize isolated patch interiors.

Slightly negative snow-cover dNDVI slopes were observed in the first 11–19 years post-fire, indicating a continued loss of conifer vegetation greenness across forest types. Although most trees are killed directly by wildfire, mortality may continue for several years from increased abiotic stressors, insect infestations, or fire injuries (Hood and Varner, 2020). Fir-spruce may have seen a longer period of negative slope due to increased post-fire mortality from greater sensitivity to fire-injury

Table 3
Odds-ratios derived from the generalized linear logistic regression model of conifer recovery. Odds-ratios greater than one indicate an increased likelihood of high-severity burn patch achieving 80% conifer recolonization 30 years post-fire, where values less than one indicate a reduced likelihood of recovery. Categorical predictors show the relative difference in odds between each pairwise comparison, with the same odds reported for both ratios. Continuous predictors show the odds-ratio as the change in recovery likelihood for a one unit increase of that predictor. The interquartile range (IQR) odds-ratio shows the change in odds of conifer recovery across the interquartile range of that variable to provide more relevant comparisons between predictors across the study area.

Predictors			Effects				
Type	Variable	Variable IQR	Odds-Ratio	Odds-Ratio 95% CI	IQR Odds-Ratio	IQR Odds-Ratio 95% CI	*p*
Forest Type	Douglas-Fir - Fir-Spruce	–	1.999	[1.432, 2.791]	1.999	[1.432, 2.791]	<0.0001
Forest Type	Lodgepole Pine - Fir-Spruce	–	6.002	[4.967, 7.252]	6.002	[4.967, 7.252]	<0.0001
Forest Type	Lodgepole Pine - Douglas-Fir	–	3.002	[2.167, 4.158]	3.002	[2.167, 4.158]	<0.0001
Climate	Climatic Water Deficit (DEF; mm)	17.77–22.02	0.958	[0.940, 0.976]	0.833	[0.769, 0.902]	<0.001
Patch	Patch Area (ha)	3.42–18.02	0.999	[0.999, 1.000]	0.999	[0.997, 1.001]	>0.05
Patch	Area to Perimeter Ratio (ha/m)	30.27–51.64	0.992	[0.988, 0.995]	0.838	[0.774, 0.908]	<0.0001
Topography	Elevation (m)	2267-2596	0.997	[0.996, 0.997]	0.356	[0.313, 0.406]	<0.0001
Topography	Slope (degrees)	6.48–19.05	0.899	[0.887, 0.911]	0.263	[0.225, 0.309]	<0.0001
Topography	Aspect (cos(radians))	−0.46-0.49	1.635	[1.408, 1.899]	1.589	[1.379, 1.829]	<0.0001

(DeNitto et al., 2000) or greater snag longevity in thin-barked Engelmann spruce and subalpine fir (Everett et al., 1999; Russell et al., 2006). Variation in snow-cover dNDVI detection points, when conifer vegetation greenness begins to increase, likely results from differing stand development timelines and snow depth. Although detection lags are common in approaches to separate vegetation types (Kiel and Turner, 2022), accounting for the multi-year lag between seedling establishment and detection is important when interpreting vegetation recovery using snow cover imagery. Greater accumulated snow depth and slower tree growth rates likely lengthen the time required for conifer seedlings to reach a detectable height above the snowpack by obscuring visible NDVI signals. Fir-spruce likely had the longest time to dNDVI detection, with prolonged seedling establishment and slow growth rates (Ferguson and Carlson, 2010) paired with greater snow depths in higher elevation forests (Grundstein and Mote, 2010). Detection occurred sooner within lodgepole pine and Douglas-fir, which are typically found at lower elevations with relatively faster growth rates (Ferguson and Carlson, 2010).

The recovery timelines we estimated from snow-cover NDVI are longer than those reported in similar studies evaluating growing-season spectral recovery (Bright et al., 2019). Previous application of snow-cover imagery has found similar discrepancies, showing that growing-season NDVI estimated post-fire recovery nearly five times sooner than with snow-cover NDVI over a wide range of burn severities and forest types (Vanderhoof et al., 2021). The non-specific nature of growing-season NDVI hinders the evaluation of early post-fire regrowth, which tends to be largely dominated by deciduous and herbaceous cover. Reduced conifer establishment may be associated with competition from early-seral aspen dominance (St. Clair et al., 2013) or compensatory increases in shrub and herbaceous biomass (Kiel and Turner, 2022), further obscuring recovery trends. Mischaracterizing or overestimating forest recovery presents challenges to direct management efforts, evaluate wildfire impacts, monitor aboveground carbon storage, and identify areas of landscape conversion to non-forest vegetation. Techniques to spectrally separate vegetation types provide an opportunity to address these challenges and better characterize post-fire recovery across conifer-dominated forest ecosystems.

4.3. Characteristics of conifer recovery and implications for resilience

Although our analyses documented general patterns of conifer recovery following high-severity wildfires in the Northern Rocky Mountains, we found that 35% of our study area was not recolonized by coniferous vegetation after 30 years. Areas of persistent regeneration failure are at risk of conversion to non-forest vegetation communities and indicate reduced resilience to high-severity wildfire. Variables associated with conifer regeneration success can be used to identify locations within high-severity events that may be at greater risk of regeneration failure, appropriately direct management efforts, and evaluate consequences of shifting wildfire regimes. Although our analysis considered multiple fire events, the relatively distinct time period of the fires evaluated should be considered in interpreting results.

Fir-spruce forests had relatively poor likelihoods of conifer recovery relative to Douglas-fir and lodgepole pine, aligning with the snow-cover dNDVI trends and modeled proportions of conifer recolonization. Slower establishment, growth, and seed production constrain fir-spruce recovery, limiting the ability of conifer trees to effectively recolonize high-severity burn patches within 30 years. Our characterization of protracted post-fire recovery within fir-spruce forests is supported by other field-based assessments of post-fire regeneration (Harvey et al., 2016a; Stevens-Rumann et al., 2018). Historically, slower post-fire recovery within fir-spruce forests has maintained resilience with a fire regime of infrequent (>200 years), high-severity events (Schoennagel et al., 2004). Increasing wildfire extent and shortening return intervals within subalpine forests may, however, pose challenges for future forest recovery (Gill et al., 2021; Harvey et al., 2016b; Stevens-Rumann and Morgan, 2016). Douglas-fir and lodgepole pine exhibited comparably greater recovery, with remaining unforested areas concentrated within a few, larger patches, aligning with prior field studies (Kiel and Turner, 2022). Areas of regeneration failure were particularly concentrated within lodgepole pine forests, where the median patch is 100% forested, yet 28% of the total area is absent of conifer trees. Although recovery was comparably greater for Douglas-fir and lodgepole pine, large areas of regeneration failure are ecologically significant and consequential to post-fire management efforts.

Characteristics of high-severity burn patches that limited seed dispersal or challenged seedling success were also associated with reduced likelihoods of conifer recovery. High-severity burn patches located in drier environments and topographic extremes were associated with decreasing likelihoods of conifer recovery. Topography and climate have been shown to impact recovery by creating site conditions adverse to seedling success or limiting seed dispersal capacity (Harvey et al., 2016a; Kemp et al., 2019; Kiel and Turner, 2022; Stevens-Rumann et al., 2018). Decreased conifer recovery was also associated with larger patch area-to-perimeter ratios. Patch area-to-perimeter ratios provide more information than patch size alone by considering the spatial arrangement of the burned area. Patches with high area-to-perimeter ratios (i.e., circular) may inhibit seed dispersal by having a smaller proportion of burned area near a patch edge and surviving parent trees. The influence of patch area-to-perimeter ratios indicates that the negative impact of increasing patch size on forest recovery may be somewhat mitigated by spatial configurations that support seed dispersal. The importance of patch configuration aligns with prior field-based research showing that landscape heterogeneity has been important to maintain post-fire resilience in the Northern Rocky Mountains (Clark-Wolf et al., 2022;

Harvey et al., 2016b; Kemp et al., 2016; Kiel and Turner, 2022) and specifically supported post-fire recovery in fires used in our analysis (Schoennagel et al., 2008; Turner et al., 1999). With anticipated declines in burn severity heterogeneity in the Northern Rockies (Harvey et al., 2016b) and shifting climate conditions (Abatzoglou and Williams, 2016), our findings suggest that forest resilience may be eroded by increased prevalence of high-severity wildfires.

5. Conclusions

Our study demonstrates that snow-cover Landsat imagery can be successfully utilized to evaluate conifer-specific vegetation recovery following high-severity fire. Consistent with previous research, we found that snow-cover NDVI is an effective method to track post-fire conifer regeneration at a landscape scale, produce ecologically consistent results, and avoid confusion with herbaceous vegetation that can occur when using growing-season imagery. Our study is the first to outline snow-cover Landsat detectability limits and utilize remotely-sensed snow-cover imagery to spatially model the presence of conifer regeneration. >98% detection accuracy was achieved for identifying conifer regeneration presence in a Landsat pixel, with the preponderance of misclassified conifer-absent pixels having <10% conifer cover. Such high model reliability suggests that snow-cover remote sensing can be used to provide a clearer picture of post-fire regeneration dynamics and better evaluate post-fire forest recovery. Applying our methodologies to a wide range of fire events could provide valuable insight into the long-term trends and variations in post-fire conifer regeneration across fire-prone forest ecosystems.

We were able to employ snow-cover remote sensing to model conifer-specific vegetation recovery for nearly 300,000 ha burned at high-severity. By focusing on conifer-specific forest regrowth, we gain a clearer understanding of post-fire recovery dynamics and can better evaluate strategies for addressing the ecological implications of high-severity fire. Our research has constructed a more detailed picture of long-term post-fire forest recovery for lodgepole pine, Douglas-fir, and fir-spruce forests in the Northern Rocky Mountains, demonstrating differences in the rate and pattern of conifer recolonization. We identified patch-level characteristics associated with reduced likelihoods of conifer recovery, underlining the importance of environmental conditions and heterogeneity in supporting forest resilience. Understanding conifer recovery patterns and controls following high-severity wildfires is crucial for addressing the challenges posed by increasing wildfire occurrence, extent, and severity.

CRediT authorship contribution statement

Casey Menick: Writing – original draft, Methodology, Formal analysis, Conceptualization. **Wade Tinkham:** Writing – review & editing, Supervision, Methodology, Funding acquisition, Conceptualization. **Chad Hoffman:** Writing – review & editing, Methodology, Conceptualization. **Melanie Vanderhoof:** Writing – review & editing, Methodology, Conceptualization. **Jody Vogeler:** Writing – review & editing, Methodology, Conceptualization.

Declaration of competing interest

The authors declare that they have no known competing financial interests or personal relationships that could have appeared to influence the work reported in this paper.

Data availability

Data will be made available on request.

Acknowledgment

This research was initiated as part of the NASA DEVELOP node at Colorado State University and was supported in part by the USDA Rocky Mountain Research Station Joint Venture Agreement (20-JV-11221633-140). This research was supported by the USDA Forest Service, Rocky Mountain Research Station, as well as the U.S. Geological Survey's National Land Imaging and Land Change Science Programs. We appreciate comments on earlier versions from Doug Shinneman. The findings and conclusions in this publication are those of the authors and should not be construed to represent any official USDA determination or policy. Any use of trade, firm, or product names is for descriptive purposes only and does not imply endorsement by the U.S. Government.

References

Abatzoglou, J.T., Williams, A.P., 2016. Impact of anthropogenic climate change on wildfire across western US forests. Proc. Natl. Acad. Sci. 113 (42), 11770–11775. https://doi.org/10.1073/pnas.1607171113.

Abatzoglou, J.T., Dobrowski, S.Z., Parks, S.A., Hegewisch, K.C., 2018. TerraClimate, a high-resolution global dataset of monthly climate and climatic water balance from 1958-2015. Sci. Data 5 (1), 1–12. https://doi.org/10.1038/sdata.2017.191.

Ackers, S.H., Davis, R.J., Olsen, K.A., Dugger, K.M., 2015. The evolution of mapping habitat for northern spotted owls (*Strix occidentalis caurina*): a comparison of photo-interpreted, Landsat-based, and lidar-based habitat maps. Remote Sens. Environ. 156, 361–373. https://doi.org/10.1016/j.rse.2014.09.025.

Bartels, S.F., Chen, H.Y.H., Wulder, M.A., White, J.C., 2016. Trends in post-disturbance recovery rates of Canada's forests following wildfire and harvest. For. Ecol. Manag. 361, 194–207. https://doi.org/10.1016/j.foreco.2015.11.015.

Bayham, J., Yoder, J.K., Champ, P.A., Calkin, D.E., 2022. The economics of wildfire in the United States. Ann. Rev. Resour. Econ. 14, 379–401. https://doi.org/10.1146/annurev-resource-111920.

Belgiu, M., Drăguţ, L., 2016. Random forest in remote sensing: a review of applications and future directions. ISPRS J. Photogramm. Remote Sens. 114, 24–31. https://doi.org/10.1016/j.isprsjprs.2016.01.011.

Bolton, D.K., Coops, N.C., Wulder, M.A., 2015. Characterizing residual structure and forest recovery following high-severity fire in the western boreal of Canada using Landsat time-series and airborne lidar data. Remote Sens. Environ. 163, 48–60. https://doi.org/10.1016/j.rse.2015.03.004.

Bright, B.C., Hudak, A.T., Kennedy, R.E., Braaten, J.D., Henareh Khalyani, A., 2019. Examining post-fire vegetation recovery with Landsat time series analysis in three western north American forest types. Fire Ecol. 15 (1) https://doi.org/10.1186/s42408-018-0021-9.

Cansler, C.A., McKenzie, D., 2012. How robust are burn severity indices when applied in a new region? Evaluation of alternate field-based and remote-sensing methods. Remote Sens. 4 (2), 456–483. https://doi.org/10.3390/rs4020456.

Casady, G.M., van Leeuwen, W.J., Marsh, S.E., 2010. Evaluating post-wildfire vegetation regeneration as a response to multiple environmental determinants. Environ. Model. Assess. 15, 295–307. https://doi.org/10.1007/s10666-009-9210-x.

Certini, G., 2005. Effects of fire on properties of forest soils: a review. Oecologia 143 (1), 1–10. https://doi.org/10.1007/s00442-004-1788-8.

Chambers, M.E., Fornwalt, P.J., Malone, S.L., Battaglia, M.A., 2016. Patterns of conifer regeneration following high severity wildfire in ponderosa pine-dominated forests of the Colorado front range. For. Ecol. Manag. 378, 57–67. https://doi.org/10.1016/j.foreco.2016.07.001.

Chen, W., Moriya, K., Sakai, T., Koyama, L., Cao, C., 2014. Monitoring of post-fire forest recovery under different restoration modes based on time series Landsat data. European J. Remote Sens. 47 (1), 153–168. https://doi.org/10.5721/eujrs20144710.

Chuvieco, E., Aguado, I., Salas, J., García, M., Yebra, M., Oliva, P., 2020. Satellite remote sensing contributions to wildland fire science and management. Curr. For. Rep. 6, 81–96. https://doi.org/10.1007/s40725-020-00116-5.

Clark-Wolf, K., Higuera, P.E., Davis, K.T., 2022. Conifer seedling demography reveals mechanisms of initial forest resilience to wildfires in the northern Rocky Mountains. For. Ecol. Manag. 523 https://doi.org/10.1016/j.foreco.2022.120487.

Collins, B.M., Stephens, S.L., 2010. Stand-replacing patches within a "mixed severity" fire regime: quantitative characterization using recent fires in a long-established natural fire area. Landsc. Ecol. 25 (6), 927–939. https://doi.org/10.1007/s10980-010-9470-5.

Daubenmire, R.F., 1943. Vegetational zonation in the Rocky Mountains. Bot. Rev. 9 (6), 325–393. https://doi.org/10.1007/BF02872481.

Davis, K.T., Dobrowski, S.Z., Higuera, P.E., Holden, Z.A., Veblen, T.T., Rother, M.T., Parks, S.A., Sala, A., Maneta, M.P., 2019. Wildfires and climate change push low-elevation forests across a critical climate threshold for tree regeneration. Proc. Natl. Acad. Sci. 116 (13), 6193–6198. https://doi.org/10.5061/dryad.pc3f9d8.

DeNitto, G., Cramer, B., Gibson, K., Lockman, B., McConnell, T., Stipe, L., 2000. Survivability and Deterioration of Fire-Injured Trees in the Northern Rocky Mountains: A Review of the Literature. The Bark Beetles, Fuels, and Fire Bibliography, p. 1.

Dennison, P.E., Brewer, S.C., Arnold, J.D., Moritz, M.A., 2014. Large wildfire trends in the western United States, 1984-2011. Geophys. Res. Lett. 41 (8), 2928–2933. https://doi.org/10.1002/2014GL059576.

Donato, D.C., Harvey, B.J., Turner, M.G., 2016. Regeneration of montane forests 24 years after the 1988 Yellowstone fires: a fire-catalyzed shift in lower treelines? Ecosphere 7 (8). https://doi.org/10.1002/ecs2.1410.

Dymond, C.C., Mladenoff, D.J., Radeloff, V.C., 2002. Phenological differences in tasseled cap indices improve deciduous forest classification. Remote Sens. Environ. 80 (3), 460–472. https://doi.org/10.1016/S0034-4257(01)00324-8.

Eidenshink, J., Schwind, B., Brewer, K., Zhu, Z.-L., Quayle, B., Howard, S., 2007. A project for monitoring trends in burn severity. Fire Ecol. 3 (1), 3–21. https://doi.org/10.4996/fireecology.0301003.

Englin, J., Boxall, P.C., Chakraborty, K., Watson, D.O., 1996. Valuing the impacts of forest fires on backcountry forest recreation. For. Sci. 42 (4), 450–455. https://doi.org/10.1093/forestscience/42.4.450.

Everett, R., Lehmkuhl, J., Schellhaas, R., Ohlson, P., Keenum, D., Riesterer, H., Spurbeck, D., 1999. Snag dynamics in a chronosequence of 26 wildfires on the east slope of the Cascade Range in Washington state, USA. Int. J. Wildland Fire 9 (4), 223–234. https://doi.org/10.1071/wf00011.

Ferguson, D.E., Carlson, C.E., 2010. Height-Age Relationships for Regeneration-Size Trees in the Northern Rocky Mountains. US Department of Agriculture, Forest Service, Rocky Mountain Research Station, USA.

Flannigan, M.D., Krawchuk, M.A., de Groot, W.J., Wotton, B.M., Gowman, L.M., 2009. Implications of changing climate for global wildland fire. Int. J. Wildland Fire 18 (5), 483–507. https://doi.org/10.1071/WF08187.

Fontaine, J.B., Kennedy, P.L., 2012. Meta-analysis of avian and small-mammal response to fire severity and fire surrogate treatments in US fire-prone forests. Ecol. Appl. 22 (5), 1547–1561. https://doi.org/10.1890/12-0009.1.

Food and Agriculture Organization of the United Nations, 2020. Global Forest Resources Assessment, terms and Definitions, 188. Forest Resources Assessment Working Paper, p. 32.

Frazier, R.J., Coops, N.C., Wulder, M.A., Hermosilla, T., White, J.C., 2018. Analyzing spatial and temporal variability in short-term rates of post-fire vegetation return from Landsat time series. Remote Sens. Environ. 205, 32–45. https://doi.org/10.1016/j.rse.2017.11.007.

Gao, B.-C., 1996. NDWI - a normalized difference water index for remote sensing of vegetation liquid water from space. Remote Sens. Environ. 58 (3), 257–266. https://doi.org/10.1016/S0034-4257(96)00067-3.

García, M.J.L., Caselles, V., 1991. Mapping burns and natural reforestation using thematic mapper data. Geocarto. Int. 6 (1), 31–37. https://doi.org/10.1080/10106049109354290.

Gellman, J., Walls, M., Wibbenmeyer, M., 2022. Wildfire, smoke, and outdoor recreation in the western United States. Forest Policy Econ. 134 https://doi.org/10.1016/j.forpol.2021.102619.

Gill, N.S., Hoecker, T.J., Turner, M.G., 2021. The propagule doesn't fall far from the tree, especially after short-interval, high-severity fire. Ecology 102 (1). https://doi.org/10.1002/ecy.3194.

Girvetz, E.H., Greco, S.E., 2007. How to define a patch: a spatial model for hierarchically delineating organism-specific habitat patches. Landsc. Ecol. 22 (8), 1131–1142. https://doi.org/10.1007/s10980-007-9104-8.

Gray, A.N., Brandeis, T.J., Shaw, J.D., McWilliams, W.H., Miles, P.D., 2012. Forest inventory and analysis database of the United States of America (FIA). Biodiversit. Ecol. 4, 225–231.

Grundstein, A., Mote, T., 2010. Trends in average snow depth across the Western United States. Phys. Geogr. 31 (2), 172–185. https://doi.org/10.2747/0272-3646.31.2.172.

Haffey, C., Sisk, T.D., Allen, C.D., Thode, A.E., Margolis, E.Q., 2018. Limits to ponderosa pine regeneration following large high-severity forest fires in the United States southwest. Fire Ecol. 14 (1), 143–163. https://doi.org/10.4996/fireecology.140114316.

Hall, D.K., Riggs, G.A., 2010. Normalized-difference snow index (NDSI). In: Encyclopedia of Snow, Ice and Glaciers. https://doi.org/10.1007/978-90-481-2642-2_376.

Hall, D.K., Riggs, G.A., Salomonson, V.V., 1995. Development of methods for mapping global snow cover using moderate resolution imaging spectroradiometer data. Remote Sens. Environ. 54 (2), 127–140. https://doi.org/10.1016/0034-4257(95)00137-P.

Hanson, C.T., Odion, D.C., 2014. Is fire severity increasing in the Sierra Nevada, California, USA? Int. J. Wildland Fire 23 (1), 1–8. https://doi.org/10.1071/WF13016.

Harrell Jr., F., 2013. rms: Regression Modeling Strategies. R Package VERSION, 5(2).

Harvey, B.J., Donato, D.C., Turner, M.G., 2016a. Burn me twice, shame on who? Interactions between successive forest fires across a temperate mountain region. Ecology 97 (9), 2272–2282. https://doi.org/10.1002/ecy.1439.

Harvey, B.J., Donato, D.C., Turner, M.G., 2016b. Drivers and trends in landscape patterns of stand-replacing fire in forests of the US northern Rocky Mountains (1984–2010). Landsc. Ecol. 31 (10), 2367–2383. https://doi.org/10.1007/s10980-016-0408-4.

Harvey, B.J., Donato, D.C., Turner, M.G., 2016c. High and dry: post-fire tree seedling establishment in subalpine forests decreases with post-fire drought and large stand-replacing burn patches. Glob. Ecol. Biogeogr. 25 (6), 655–669. https://doi.org/10.1111/geb.12443.

Holden, Z.A., Morgan, P., Smith, A.M., Vierling, L., 2010. Beyond Landsat: a comparison of four satellite sensors for detecting burn severity in ponderosa pine forests of the Gila wilderness, NM, USA. Int. J. Wildland Fire 19 (4), 449–458. https://doi.org/10.1071/wf07106.

Hollister, J., Shah, T., Robitaille, A., Beck, M., Johnson, M., 2021. Elevatr: Access Elevation Data from Various APIs. https://doi.org/10.5281/zenodo.5809645.

Hood, S.M., Varner, J.M., 2020. Post-fire Tree Mortality. Encyclopedia of Wildfires and Wildland-Urban Interface (WUI) Fires, pp. 836–844. https://doi.org/10.1007/978-3-319-51727-8_252-1.

Howe, A.A., Parks, S.A., Harvey, B.J., Saberi, S.J., Lutz, J.A., Yocom, L.L., 2022. Comparing Sentinel-2 and Landsat 8 for burn severity mapping in Western North America. Remote Sens. 14 (20), 5249. https://doi.org/10.3390/rs14205249.

Huete, A., Didan, K., Miura, T., Rodriguez, E.P., Gao, X., Ferreira, L.G., 2002. Overview of the radiometric and biophysical performance of the MODIS vegetation indices. Remote Sens. Environ. 83, 195–213. https://doi.org/10.1016/S0034-4257(02)00096-2.

Ice, G.G., Neary, D.G., Adams, P.W., 2004. Effects of wildfire on soils and watershed processes. J. For. 102 (6), 16–20. https://doi.org/10.1093/jof/102.6.16.

Jolly, W.M., Cochrane, M.A., Freeborn, P.H., Holden, Z.A., Brown, T.J., Williamson, G.J., Bowman, D.M.J.S., 2015. Climate-induced variations in global wildfire danger from 1979 to 2013. Nat. Commun. 6 https://doi.org/10.1038/ncomms8537.

Kashian, D.M., Tinker, D.B., Turner, M.G., Scarpace, F.L., 2004. Spatial heterogeneity of lodgepole pine sapling densities following the 1988 fires in Yellowstone National Park, Wyoming, USA. Can. J. For. Res. 34 (11), 2263–2276. https://doi.org/10.1139/X04-107.

Kashian, D.M., Romme, W.H., Tinker, D.B., Turner, M.G., Ryan, M.G., 2006. Carbon storage on landscapes with stand-replacing fires. Bioscience 56 (7), 598–606. https://doi.org/10.1641/0006-3568(2006)56[598:CSOLWS]2.0.CO;2.

Kattenborn, T., Schiefer, F., Frey, J., Feilhauer, H., Mahecha, M.D., Dormann, C.F., 2022. Spatially autocorrelated training and validation samples inflate performance assessment of convolutional neural networks. ISPRS Open J. Photogrammet. Remote Sens. 5, 100018 https://doi.org/10.1016/j.ophoto.2022.100018.

Kemp, K.B., Higuera, P.E., Morgan, P., 2016. Fire legacies impact conifer regeneration across environmental gradients in the U.S. northern Rockies. Landsc. Ecol. 31 (3), 619–636. https://doi.org/10.1007/s10980-015-0268-3.

Kemp, K.B., Higuera, P.E., Morgan, P., Abatzoglou, J.T., 2019. Climate will increasingly determine post-fire tree regeneration success in low-elevation forests, northern Rockies, USA. Ecosphere 10 (1). https://doi.org/10.1002/ecs2.2568.

Key, C.H., Benson, N.C., 2006. Landscape assessment (LA). FIREMON: fire effects monitoring and inventory system. In: Gen. Tech. Rep. RMRS-GTR-164-CD, Fort Collins, CO: US Department of Agriculture, Forest Service, Rocky Mountain Research Station.

Kiel, N.G., Turner, M.G., 2022. Where are the trees? Extent, configuration, and drivers of poor forest recovery 30 years after the 1988 Yellowstone fires. For. Ecol. Manag. 524 https://doi.org/10.1016/j.foreco.2022.120536.

Kolden, C.A., Smith, A.M.S., Abatzoglou, J.T., 2015. Limitations and utilisation of monitoring trends in burn severity products for assessing wildfire severity in the USA. Int. J. Wildland Fire 24 (7), 1023–1028. https://doi.org/10.1071/WF15082.

Lannom, K.O., Tinkham, W.T., Smith, A.M.S., Abatzoglou, J., Newingham, B.A., Hall, T.E., Morgan, P., Strand, E.K., Paveglio, T.B., Anderson, J.W., Sparks, A.M., 2014. Defining extreme wildland fires using geospatial and ancillary metrics. Int. J. Wildland Fire 23 (3), 322–337. https://doi.org/10.1071/WF13065.

Liaw, A., Wiener, M., 2002. Classification and regression by randomForest. R News 2 (3), 18–22.

Loehman, R.A., 2020. Drivers of wildfire carbon emissions. Nat. Clim. Chang. 10 (12), 1070–1071. https://doi.org/10.1038/s41558-020-00922-6.

McCarley, T.R., Kolden, C.A., Vaillant, N.M., Hudak, A.T., Smith, A.M.S., Wing, B.M., Kellogg, B.S., Kreitler, J., 2017. Multi-temporal LiDAR and Landsat quantification of fire-induced changes to forest structure. Remote Sens. Environ. 191, 419–432. https://doi.org/10.1016/j.rse.2016.12.022.

Meigs, G.W., Donato, D.C., Campbell, J.L., Martin, J.G., Law, B.E., 2009. Forest fire impacts on carbon uptake, storage, and emission: the role of burn severity in the eastern cascades, Oregon. Ecosystems 12, 1246–1267. https://doi.org/10.1007/s10021-009-9285-x.

Miller, J.D., Thode, A.E., 2007. Quantifying burn severity in a heterogeneous landscape with a relative version of the delta normalized burn ratio (dNBR). Remote Sens. Environ. 109 (1), 66–80. https://doi.org/10.1016/j.rse.2006.12.006.

Miller, J.D., Knapp, E.E., Key, C.H., Skinner, C.N., Isbell, C.J., Creasy, R.M., Sherlock, J.W., 2009. Calibration and validation of the relative differenced normalized burn ratio (RdNBR) to three measures of fire severity in the Sierra Nevada and Klamath Mountains, California, USA. Remote Sens. Environ. 113 (3), 645–656. https://doi.org/10.1016/j.rse.2008.11.009.

Miller, J.D., Skinner, C.N., Safford, H.D., Knapp, E.E., Ramirez, C.M., 2012. Trends and causes of severity, size, and number of fires in northwestern California, USA. Ecol. Appl. 22 (1), 184–203. https://doi.org/10.1890/10-2108.1.

Morgan, P., Heyerdahl, E.K., Gibson, C.E., 2008. Multi-season climate synchronized forest fires throughout the 20th century, northern Rockies, USA. Ecology 89 (3), 717–728. https://doi.org/10.1890/06-2049.1.

Morresi, D., Vitali, A., Urbinati, C., Garbarino, M., 2019. Forest spectral recovery and regeneration dynamics in stand-replacing wildfires of central Apennines derived from Landsat time series. Remote Sens. 11 (3), 308. https://doi.org/10.3390/rs11030308.

Muggeo, V.M., 2008. Segmented: an R package to fit regression models with broken-line relationships. R News 8 (1), 20–25.

Myneni, R.B., Hall, F.G., Sellers, P.J., Marshak, A.L., 1995. The interpretation of spectral vegetation indexes. IEEE Trans. Geosci. Remote Sens. 33 (2), 481–486. https://doi.org/10.1109/36.377948.

Negrón-Juárez, R.I., Chambers, J.Q., Marra, D.M., Ribeiro, G.H.P.M., Rifai, S.W., Higuchi, N., Roberts, D., 2011. Detection of subpixel treefall gaps with Landsat imagery in Central Amazon forests. Remote Sens. Environ. 115 (12), 3322–3328. https://doi.org/10.1016/j.rse.2011.07.015.

Nelson, M.D., Buech, R.R., 1996. A test of 3 models of Kirtland's warbler habitat suitability. Wildl. Soc. Bull. 89–97.
Niemeyer, R.J., Bladon, K.D., Woodsmith, R.D., 2020. Long-term hydrologic recovery after wildfire and post-fire forest management in the interior Pacific northwest. Hydrol. Process. 34 (5), 1182–1197. https://doi.org/10.1002/hyp.13665.
Obata, S., Cieszewski, C.J., Lowe, R.C., Bettinger, P., 2021. Random Forest regression model for estimation of the growing stock volumes in Georgia, USA, using dense Landsat time series and FIA dataset. Remote Sens. 13 (2), 1–18. https://doi.org/10.3390/rs13020218.
O'Donnell, F.C., Flatley, W.T., Springer, A.E., Fulé, P.Z., 2018. Forest restoration as a strategy to mitigate climate impacts on wildfire, vegetation, and water in semiarid forests. Ecol. Appl. 28 (6), 1459–1472. https://doi.org/10.1002/eap.1746.
Olofsson, P., Foody, G.M., Herold, M., Stehman, S.V., Woodcock, C.E., Wulder, M.A., 2014. Good practices for estimating area and assessing accuracy of land change. Remote Sens. Environ. 148, 42–57. https://doi.org/10.1016/j.rse.2014.02.015.
Omernik, J.M., Griffith, G.E., 2014. Ecoregions of the conterminous United States: evolution of a hierarchical spatial framework. Environ. Manag. 54 (6), 1249–1266. https://doi.org/10.1007/s00267-014-0364-1.
Owen, S.M., Sieg, C.H., Sánchez Meador, A.J., Fulé, P.Z., Iniguez, J.M., Baggett, L.S., Fornwalt, P.J., Battaglia, M.A., 2017. Spatial patterns of ponderosa pine regeneration in high-severity burn patches. For. Ecol. Manag. 405, 134–149. https://doi.org/10.1016/j.foreco.2017.09.005.
Parks, S.A., Abatzoglou, J.T., 2020. Warmer and drier fire seasons contribute to increases in area burned at high severity in Western US forests from 1985 to 2017. Geophys. Res. Lett. 47 (22) https://doi.org/10.1029/2020GL089858.
Parks, S.A., Holsinger, L.M., Voss, M.A., Loehman, R.A., Robinson, N.P., 2018. Mean composite fire severity metrics computed with google earth engine offer improved accuracy and expanded mapping potential. Remote Sens. 10 (6) https://doi.org/10.3390/rs10060879.
Parks, S.A., Dobrowski, S.Z., Shaw, J.D., Miller, C., 2019. Living on the edge: trailing edge forests at risk of fire-facilitated conversion to non-forest. Ecosphere 10 (3). https://doi.org/10.1002/ecs2.2651.
Pelletier, F., Eskelson, B.N.I., Monleon, V.J., Tseng, Y.C., 2021. Using landsat imagery to assess burn severity of national forest inventory plots. Remote Sens. 13 (10) https://doi.org/10.3390/rs13101935.
Picotte, J.J., Peterson, B., Meier, G., Howard, S.M., 2016. 1984-2010 trends in fire burn severity and area for the conterminous US. Int. J. Wildland Fire 25 (4), 413–420. https://doi.org/10.1071/WF15039.
Prichard, S.J., Stevens-Rumann, C.S., Hessburg, P.F., 2017. Tamm review: shifting global fire regimes: lessons from reburns and research needs. For. Ecol. Manag. 396, 217–233. https://doi.org/10.1016/j.foreco.2017.03.035.
R Core Team, 2021. R: A Language and Environment for Statistical Computing. R Foundation for Statistical Computing, Vienna, Austria.
Riggs, G.A., Hall, D.K., Román, M.O., 2017. Overview of NASA's MODIS and visible infrared imaging radiometer suite (VIIRS) snow-cover earth system data records. Earth Syst. Sci. Data 9 (2), 765–777.
Riley, K.L., Loehman, R.A., 2016. Mid-21st century climate changes increase predicted fire occurrence and fire season length, northern Rocky Mountains, United States. Ecosphere 7 (11). https://doi.org/10.1002/ecs2.1543.
Ruefenacht, B., Finco, M.V., Nelson, M.D., Czaplewski, R., Helmer, E.H., Blackard, J.A., Holden, G.R., Lister, A.J., Salajanu, D., Weyermann, D., Winterberger, K., 2008. Conterminous US and Alaska forest type mapping using forest inventory and analysis data. Photogramm. Eng. Remote Sens. 74 (11), 1379–1388. https://doi.org/10.14358/PERS.74.11.1379.
Russell, R.E., Saab, V.A., Dudley, J.G., Rotella, J.J., 2006. Snag longevity in relation to wildfire and postfire salvage logging. For. Ecol. Manag. 232 (1–3), 179–187. https://doi.org/10.1016/j.foreco.2006.05.068.
Sankey, T., Glenn, N., 2011. Landsat-5 TM and lidar fusion for sub-pixel juniper tree cover estimates in a Western rangeland. Photogramm. Eng. Remote. Sens. 77 (12), 1241. https://doi.org/10.14358/PERS.77.12.1241.
Schoennagel, T., Veblen, T.T., Romme, W.H., 2004. The interaction of fire, fuels, and climate across Rocky Mountain forests. BioScience 54 (7), 661–676. https://doi.org/10.1641/0006-3568(2004)054[0661:tioffa]2.0.co;2.
Schoennagel, T., Smithwick, E.A.H., Turner, M.G., 2008. Landscape heterogeneity following large fires: insights from Yellowstone National Park, USA. Int. J. Wildland Fire 17 (6), 742–753. https://doi.org/10.1071/WF07146.
Shakesby, R.A., Doerr, S.H., 2006. Wildfire as a hydrological and geomorphological agent. Earth Sci. Rev. 74 (3–4), 269–307. https://doi.org/10.1016/j.earscirev.2005.10.006.
Sommers, W.T., Loehman, R.A., Hardy, C.C., 2014. Wildland fire emissions, carbon, and climate: science overview and knowledge needs. For. Ecol. Manag. 317, 1–8. https://doi.org/10.1016/j.foreco.2013.12.014.
Song, C., Schroeder, T.A., Cohen, W.B., 2007. Predicting temperate conifer forest successional stage distributions with multitemporal Landsat thematic mapper imagery. Remote Sens. Environ. 106 (2), 228–237. https://doi.org/10.1016/j.rse.2006.08.008.
Sparks, A.M., Boschetti, L., Tinkham, W.T., Smith, A.M.S., Lannom, K.O., Newingham, B. A., 2014. An accuracy assessment of the MTBS burned area product for shrub-steppe fires in the northern Great Basin, United States. Int. J. Wildland Fire. https://doi.org/10.1071/wf13206.
St. Clair, S.B., Cavard, X., Bergeron, Y., 2013. The role of facilitation and competition in the development and resilience of aspen forests. For. Ecol. Manag. 299, 91–99. https://doi.org/10.1016/j.foreco.2013.02.026.
Steel, Z.L., Fogg, A.M., Burnett, R., Roberts, L.J., Safford, H.D., 2022. When bigger isn't better—implications of large high-severity wildfire patches for avian diversity and community composition. Divers. Distrib. 28 (3), 439–453. https://doi.org/10.1111/ddi.13281.
Stevens, J.T., Lydersen, J.M., Collins, B.M., 2021. Appendix 4: burn severity spatial analyses. Postfire Restorat. Framework National Forests Calif. 175–182.
Stevens-Rumann, C.S., Morgan, P., 2016. Repeated wildfires alter forest recovery of mixed-conifer ecosystems. Ecol. Appl. 26 (6), 1842–1853. https://doi.org/10.1890/15-1521.1.
Stevens-Rumann, C.S., Kemp, K.B., Higuera, P.E., Harvey, B.J., Rother, M.T., Donato, D. C., Morgan, P., Veblen, T.T., 2018. Evidence for declining forest resilience to wildfires under climate change. Ecol. Lett. 21 (2), 243–252. https://doi.org/10.1111/ele.12889.
Szpakowski, D.M., Jensen, J.L.R., 2019. A review of the applications of remote sensing in fire ecology. Remote Sens. 11 (22) https://doi.org/10.3390/rs11222638.
Thapa, B., Wolter, P.T., Sturtevant, B.R., Townsend, P.A., 2020. Reconstructing past forest composition and abundance by using archived Landsat and national forest inventory data. Int. J. Remote Sens. 41 (10), 4022–4056. https://doi.org/10.1080/01431161.2019.1711245.
Thomas, D., Butry, D., Gilbert, S., Webb, D., Fung, J., 2017. The costs and losses of wildfires. NIST Spe. Publicat. 1215 (11) https://doi.org/10.6028/NIST.SP.1215.
Tinkham, W.T., Mahoney, P.R., Hudak, A.T., Domke, G.M., Falkowski, M.J., Woodall, C. W., Smith, A.M., 2018. Applications of the United States Forest inventory and analysis dataset: a review and future directions. Can. J. For. Res. 48 (11), 1251–1268. https://doi.org/10.1139/cjfr-2018-0196.
Townsend, P.A., Walsh, S.J., 2001. Remote sensing of forested wetlands: application of multitemporal and multispectral satellite imagery to determine plant community composition and structure in southeastern USA. Plant Ecol. 157, 129–149. https://doi.org/10.1023/A:1013999513172.
Trenberth, K.E., Branstator, G.W., Arkin, P.A., 1988. Origins of the 1988 north American drought. Science 242 (4886), 1640–1645. https://doi.org/10.1126/science.242.4886.1640.
Tucker, C.J., 1979. Red and photographic infrared linear combinations for monitoring vegetation. Remote Sens. Environ. 8 (2), 127–150. https://doi.org/10.1016/0034-4257(79)90013-0.
Turner, M.G., Romme, W.H., Gardner, R.H., 1999. Prefire heterogeneity, fire severity, and early postfire plant reestablishment in subalpine forests of Yellowstone national park, Wyoming. Int. J. Wildland Fire 9 (1), 21–36. https://doi.org/10.1071/wf99003.
Turner, M.G., Braziunas, K.H., Hansen, W.D., Harvey, B.J., 2019. Short-interval severe fire erodes the resilience of subalpine lodgepole pine forests. Proc. Natl. Acad. Sci. USA 166 (23), 11319–11328. https://doi.org/10.1073/pnas.1902841116.
Van Wagtendonk, J.W., Root, R.R., Key, C.H., 2004. Comparison of AVIRIS and Landsat ETM+ detection capabilities for burn severity. Remote Sens. Environ. 92 (3), 397–408. https://doi.org/10.1016/j.rse.2003.12.015.
Vanderhoof, M.K., Hawbaker, T.J., 2018. It matters when you measure it: using snow-cover normalised difference vegetation index (NDVI) to isolate post-fire conifer regeneration. Int. J. Wildland Fire 27 (12), 815–830. https://doi.org/10.1071/WF18075.
Vanderhoof, M.K., Hawbaker, T.J., Ku, A., Merriam, K., Berryman, E., Cattau, M., 2021. Tracking rates of postfire conifer regeneration vs. deciduous vegetation recovery across the western United States. Ecol. Appl. 31 (2) https://doi.org/10.1002/eap.2237.
Viana-Soto, A., García, M., Aguado, I., Salas, J., 2022. Assessing post-fire forest structure recovery by combining LiDAR data and Landsat time series in Mediterranean pine forests. Int. J. Appl. Earth Obs. Geoinf. 108, 102754 https://doi.org/10.1016/j.jag.2022.102754.
Vukomanovic, J., Steelman, T., 2019. A systematic review of relationships between mountain wildfire and ecosystem services. Landsc. Ecol. 34 (5), 1179–1194. https://doi.org/10.1007/s10980-019-00832-9.
Wang, X.Y., Wang, J., Jiang, Z.Y., Li, H.Y., Hao, X.H., 2015. An effective method for snow-cover mapping of dense coniferous forests in the upper Heihe River basin using Landsat operational land imager data. Remote Sens. 7 (12), 17246–17257. https://doi.org/10.3390/rs71215882.
Wang, C., Wang, A., Guo, D., Li, H., Zang, S., 2022. Off-peak NDVI correction to reconstruct Landsat time series for post-fire recovery in high-latitude forests. Int. J. Appl. Earth Obs. Geoinf. 107, 102754 https://doi.org/10.1016/j.jag.2022.102704.
Westerling, A.L., Hidalgo, H.G., Cayan, D.R., Swetnam, L.W., 2006. Warming and earlier spring increase Western U.S. forest wildfire activity. Science 313 (5789), 940–943. https://doi.org/10.1126/science.1128834.
Westerling, A.L., Turner, M.G., Smithwick, E.A., Romme, W.H., Ryan, M.G., 2011. Continued warming could transform greater Yellowstone fire regimes by mid-21st century. Proc. Natl. Acad. Sci. 108 (32), 13165–13170. https://doi.org/10.1073/pnas.1110199108.
White, J.D., Ryan, K.C., Key, C.C., Running, S.W., 1996. Remote sensing of forest fire severity and vegetation recovery. Int. J. Wildland Fire 6 (3), 125–136. https://doi.org/10.1071/WF9960125.
White, J.C., Wulder, M.A., Hermosilla, T., Coops, N.C., Hobart, G.W., 2017. A nationwide annual characterization of 25 years of forest disturbance and recovery for Canada using Landsat time series. Remote Sens. Environ. 194, 303–321. https://doi.org/10.1016/j.rse.2017.03.035.
White, J.C., Saarinen, N., Kankare, V., Wulder, M.A., Hermosilla, T., Coops, N.C., Pickell, P.D., Holopainen, M., Hyyppä, J., Vastaranta, M., 2018. Confirmation of post-harvest spectral recovery from Landsat time series using measures of forest cover and height derived from airborne laser scanning data. Remote Sens. Environ. 216, 262–275. https://doi.org/10.1016/j.rse.2018.07.004.

White, J.C., Hermosilla, T., Wulder, M.A., Coops, N.C., 2022. Mapping, validating, and interpreting spatio-temporal trends in post-disturbance forest recovery. Remote Sens. Environ. 271, 112904 https://doi.org/10.1016/j.rse.2022.113195.

Williams, A.P., Raymond, E., 2002. Estimation of leafy spurge cover from hyperspectral imagery using mixture tuned matched filtering. Remote Sens. Environ. 82, 446–456. https://doi.org/10.1016/S0034-4257(02)00061-5.

Wolter, P.T., Mladenoff, D.J., Host, G.E., Crow, T.R., 1995. Improved forest classification in the northern Lake states using multi-temporal Landsat imagery. Remote Sens. Environ. 210, 193–207.

Wolter, P.T., Townsend, P.A., Sturtevant, B.R., Kingdon, C.C., 2008. Remote sensing of the distribution and abundance of host species for spruce budworm in northern Minnesota and Ontario. Remote Sens. Environ. 112 (10), 3971–3982. https://doi.org/10.1016/j.rse.2008.07.005.

Wu, Z., Middleton, B., Hetzler, R., Vogel, J., Dye, D., 2015. Vegetation burn severity mapping using Landsat-8 and WorldView-2. Photogramm. Eng. Remote. Sens. 81 (2), 143–154. https://doi.org/10.14358/pers.81.2.143.

Wulder, M.A., White, J.C., Alvarez, F., Han, T., Rogan, J., Hawkes, B., 2009. Characterizing boreal forest wildfire with multi-temporal Landsat and LIDAR data. Remote Sens. Environ. 113 (7), 1540–1555. https://doi.org/10.1016/j.rse.2009.03.004.

Zhao, F.R., Meng, R., Huang, C., Zhao, M., Zhao, F.A., Gong, P., Yu, L., Zhu, Z., 2016. Long-term post-disturbance forest recovery in the greater Yellowstone ecosystem analyzed using Landsat time series stack. Remote Sens. 8 (11) https://doi.org/10.3390/rs8110898.